AD-A110 191 SRI INTERNATIONAL MENLO PARK CA F/G 14/5
PERCEPTION OF SPATIAL FEATURES WITH STEREOSCOPIC DISPLAYS.(U)
NOV 81 T P PIANTANIDA N00014-79-C-0742
UNCLASSIFIED N14-0742-81C-0002 NL

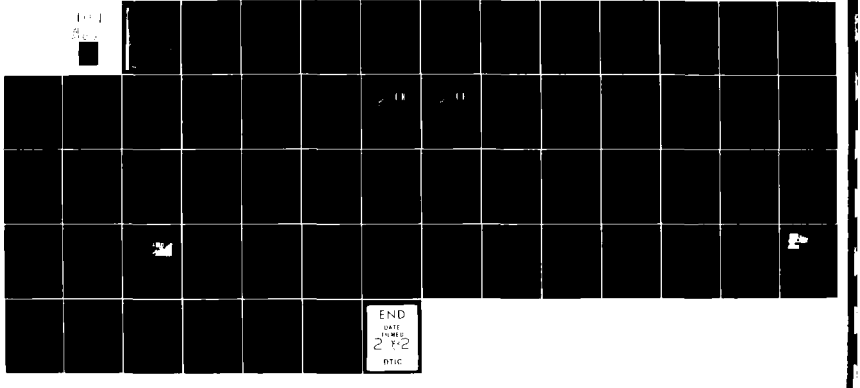

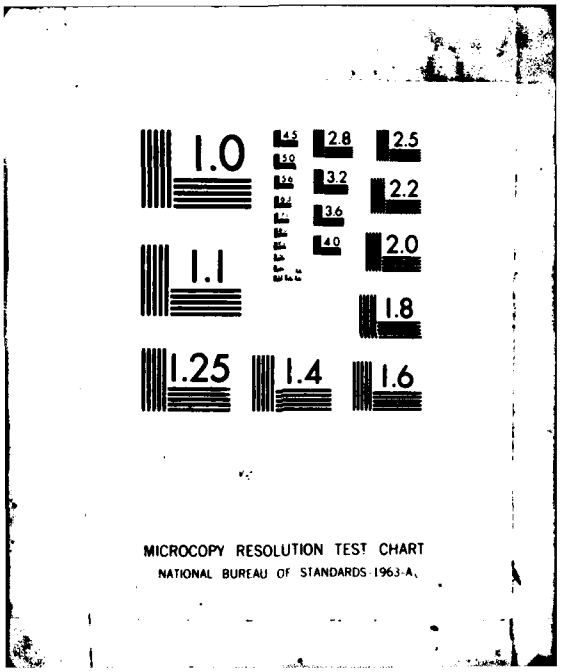
1.0
1.1
1.25
1.4
1.6
1.8
2.0
2.2
2.5
2.8
3.2
3.6
4.0
MICROCOPY RESOLUTION TEST CHART
NATIONAL BUREAU OF STANDARDS-1963-A

(12) LEVEL II

N14-0742-81C-0002

J

PERCEPTION OF SPATIAL FEATURES WITH STEREOSCOPIC DISPLAYS

Final Report

November 1981

By: Thomas P. Piantanida, Senior Research Psychologist
Bioengineering Research Center

Prepared for:

Department of the Navy
Office of Naval Research
800 North Quincy Street
Arlington, Virginia 22217

Contract N00014-79-C-0742

SRI Project 8899

SRI International
333 Ravenswood Avenue
Menlo Park, California 94025
(415) 859-6200
TWX: 910-373-2046
Telex: 334 486

Unclassified

SECURITY CLASSIFICATION OF THIS PAGE (When Data Entered)

REPORT DOCUMENTATION PAGE

READ INSTRUCTIONS BEFORE COMPLETING FORM

1. REPORT NUMBER: N14-0742-81C-0002	2. GOVT ACCESSION NO.: AD-A110 191
3. RECIPIENT'S CATALOG NUMBER:	
4. TITLE (and Subtitle): PERCEPTION OF SPATIAL FEATURES WITH STEREOSCOPIC DISPLAYS	5. TYPE OF REPORT & PERIOD COVERED: Final Report, 1 Sep 1979 — 30 Sep 1981
	6. PERFORMING ORG. REPORT NUMBER:
7. AUTHOR(s): Thomas P. Piantanida, Ph.D.	8. CONTRACT OR GRANT NUMBER(s): N00014-79-C-0742
9. PERFORMING ORGANIZATION NAME AND ADDRESS: SRI International, 333 Ravenswood Avenue, Menlo Park, California 94025	10. PROGRAM ELEMENT, PROJECT, TASK AREA & WORK UNIT NUMBERS: NR196-162
11. CONTROLLING OFFICE NAME AND ADDRESS: Office of Naval Research, Engineering Psychology Programs, 800 N. Quincy Street, Arlington, Virginia 22217	12. REPORT DATE: 30 Nov 1981; 13. NO. OF PAGES: 66
	15. SECURITY CLASS. (of this report): Unclassified
14. MONITORING AGENCY NAME & ADDRESS (if diff. from Controlling Office):	15a. DECLASSIFICATION/DOWNGRADING SCHEDULE:

16. DISTRIBUTION STATEMENT (of this report)

For public release; distribution unlimited

17. DISTRIBUTION STATEMENT (of the abstract entered in Block 20, if different from report)

18. SUPPLEMENTARY NOTES

19. KEY WORDS (Continue on reverse side if necessary and identify by block number)

Stereopsis
Depth perception
Motion-in-depth perception
Form perception
Three-dimensional displays
Stabilized images

20. ABSTRACT (Continue on reverse side if necessary and identify by block number)

This report summarizes a research program that investigated characteristics of three-dimensional displays, the effects of these characteristics on form, depth and motion-in-depth perception of human observers, and the interaction between display and observer variables. Two levels of measurement were used in this investigation: subjective measures consisting of observer responses, and objective measures consisting of observer eye movements. Two major experimental techniques were used. These were the selectively stabilized image technique, in which part of the stimulus image was stabilized on the observer's retina; and a motion-in-depth technique that allowed us to measure changes in an observer's perception of three dimensional stimuli. → next page

DD FORM 1 JAN 73 1473

EDITION OF 1 NOV 65 IS OBSOLETE

Unclassified

SECURITY CLASSIFICATION OF THIS PAGE (When Data Entered)

20. ABSTRACT (Concluded)

The major findings of this study are (1) the human stereo mechanisms responsible for the perception of depth and of motion-in-depth are sensitive to different aspects of the retinal images produced by three-dimensional displays than is the form perception mechanism; (2) it is possible to drive the human stereo mechanism with retinal images that do not drive the form perception mechanism; (3) observer variables such as ocular dominance and familiarity with three-dimensional displays interact with the three-dimensional display parameters (image luminance, image contrast, and interocular contrast), but appear not to influence the perception of motion-in-depth in three-dimensional displays during binocular image misregistration.

CONTENTS

ILLUSTRATIONS

I RATIONALE

A major effort of this study is the generation of a data base that can be used to evaluate three-dimensional display systems. Early in the course of the study a literature survey disclosed three distinct areas of information pertaining to three-dimensional display systems that required evaluation. These can be referred to as the physical aspects of three-dimensional display systems, the physiological aspects of three-dimensional (i.e., depth) perception, and observer-display interactions. Among the physical display variables, those that seemed most critical in determining perceptual quality were luminance level, luminance contrast, image motion, image bandwidth, and color. Physiological variables that affected the perception of three-dimensional display systems included retinal disparity, convergence, binocular rivalry, suppression, and fusional range. Aside from the more obvious observer-display interactions such as visual acuity relative to the spatial frequency of images on the display, astigmatism, viewing angle, viewing distance, and color perception, there were two that revealed themselves to be of some importance in predicting the probable acceptability of a given three-dimensional display system. These were ocular dominance (and the related phenomenon of binocular rivalry) and learning--that is, how familiar an observer was with the display being viewed.

Each of the physical attributes of display systems outlined above was evaluated in the course of this study. Likewise, an evaluation of the physiological variables of depth perception was also undertaken in an effort to allow more accurate prediction of the perceptual effects of various three-dimensional display parameters. In each of the experiments conducted in the course of this study, observer-display interactions were either controlled or measured by the experimenter.

II METHODS

Instrumentation

Instrumentation for this project consisted of several major pieces of apparatus, many of which were made available to the project at no cost. These include a binocular, dual-Purkinje-image eyetracker, a mirror-image pair of stimulus deflectors, a display system consisting of either a rear projection device or a computer-controlled CRT-based system, a subject response apparatus, and recording apparatus. Each of these major components is described below.

Eyetracker--Two mirror-image copies of the SRI dual-Purkinje-image eyetracker were used to monitor the position and movement of each of the observer's eyes. A schematic diagram of an eyetracker is presented in Figure 1. The principles of operation of the eyetracker are reported in Appendix A, and a synopsis of those principles is presented here.

Observers are maintained in position with respect to the eyetracker by a dental impression bite-bar. An infrared source is imaged on the observer's eye through the illumination path, and reflections of this source are captured in the collection path. The first Purkinje image (from the anterior surface of the cornea) is imaged in the center of a quadrant photocell via a servo-controlled movable mirror. Likewise, the fourth Purkinje image (from the posterior surface of the lens) is imaged in the center of another quadrant photocell by a second servo-controlled movable mirror. Relative displacements of the first and fourth Purkinje images occur with both horizontal and vertical eye movements. Analog signals corresponding to an observer's horizontal and eye movements are generated from the position of the servo-controlled mirrors in the first and fourth Purkinje-image systems. Accuracy is on the order of 1 min of arc with this system, and the field of view over which the observer's eyes can be tracked is approximately 25^{o}.

Stimulus Deflector--While fixed in position with respect to the eyetracker, observers view stimuli through a pair of stimulus deflectors. A stimulus deflector is presented diagrammatically in Figure 2 and described in detail in Appendix B. A brief description of the device will indicate how it was used in the present studies.

Each stimulus deflector consists of a pair of unity-gain relay lens systems that reimage the observer's eye in the plane of movable mirrors, one that rotates the image horizontally and another that rotates the image vertically. The axis of rotation of each mirror is in a plane conjugate to the center of rotation of the observer's eye. Therefore, rotation of the horizontal mirror, for example, results in lateral

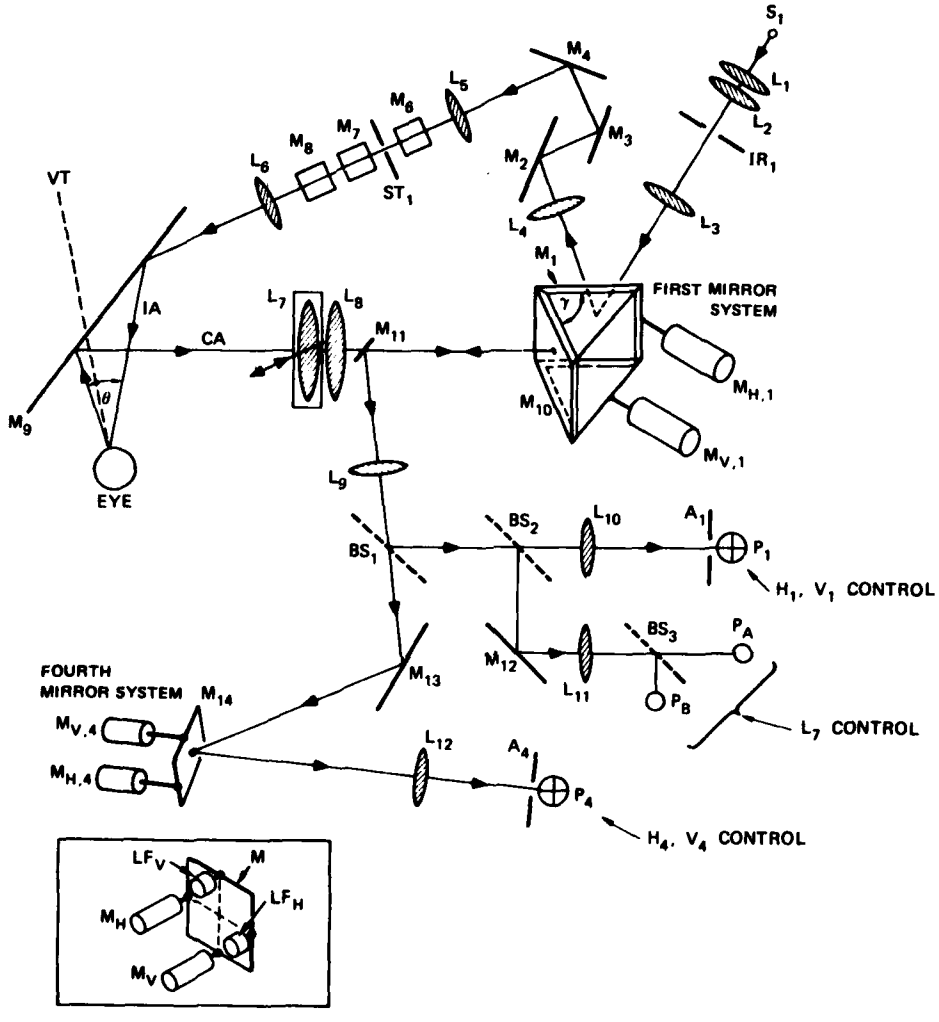

FIGURE 1 SCHEMATIC OF EYETRACKER SYSTEM

S_1, IRLED source; IR_1, adjustable iris conjugate with eye pupil; M_1 and M_{10}, coupled front-surface mirrors under control of motors $M_{H,1}$ and $M_{V,1}$; γ, angle between mirrors M_1 and M_{10}; M_2,M_3,M_4,M_6,M_7,M_8,M_{11},M_{12}, and M_{13}, front-surface mirrors (mirrors M_2,M_3,M_4, and M_5, not shown, are used in different combinations to alter the angle θ of the incoming illumination); M_{14}, front-surface mirror driven by motors $M_{V,4}$ and $M_{H,4}$;M_9, dichroic mirror; BS_1, 90/10 pellicle beam splitter; BS_2 and BS_3, 50/50 beam splitters; P_1 and P_4, quadrant photocells; A_1 and A_4, apertures in front of P_1 and P_4, respectively; P_A and P_B, photocells in automatic focus-detection circuit; VT, visual target; IA, input axis; CA, collecting axis; stop ST_1, source of Purkinje image pattern; LF_H and LF_V, linear followers.

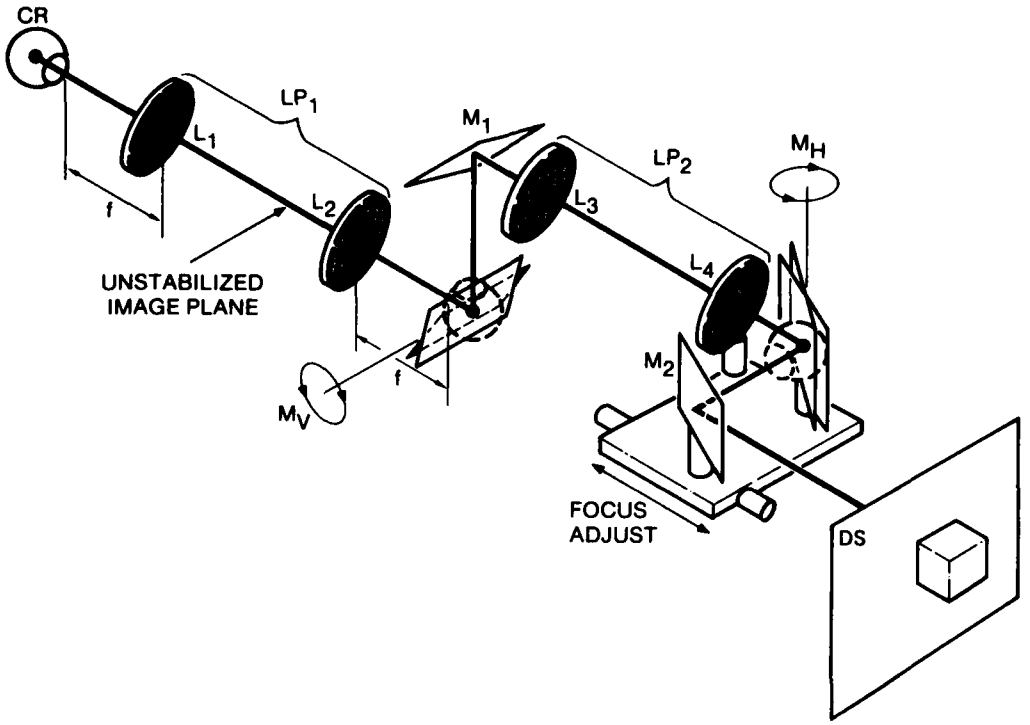

FIGURE 2 SCHEMATIC OF STIMULUS DEFLECTOR

CR, center of rotation of eye; L_1,L_2,L_3, and L_4, multiple-element camera lenses; LP, lens pair; AP, artificial pupil; DS, display screen; M_V, mirror that rotates the visual field vertically; M_H, mirror that rotates the visual field horizontally; M_1, fixed mirror; L_4,M_H, and mirror M_2 move in synchronism to adjust the optical distance to the display screen.

retinal image motion the same as would occur if the observer were to rotate his eye horizontally. A similar situation exists for the vertical stimulus-deflector mirror.

Electrical signals used to drive the horizontal and vertical stimulus-deflector mirrors may originate from any one of a number of sources. In studies designed to stabilize the retinal image, the signals that drive the horizontal stimulus-deflection mirror are derived from the horizontal eye-movement signal of the eyetracker, and the signals that drive the vertical stimulus-deflector mirror are derived from the vertical eye-movement signal from the eyetracker. In studies of unstabilized images, function generators usually provide the signals for the stimulus-deflection mirrors. Most often, the signal will be sinusoidal in voltage.

Display Systems--The studies described in this report utilized two major kinds of display systems: a rear projection system using a Kodak Carousel® projector and a computer-controlled, three-dimensional display system using two CRTs. The rear projection system was used in two modes. When it was desirable for both monocular images to be identical, the rear projection screen was illuminated by a single beam. (It was possible to present two monocular views of the stimulus, one to each of the observer's eyes, by appropriately rotating the horizontal mirror in each stimulus deflector.) When nonidentical images were to be presented to each of the observer's eyes, a rear projection system similar to that shown in Figure 3 was used. A pair of orthogonal mirrors, M_1 and M_2, separated the projection beam into two beams, and a pair of right-angle prisms redirected the beams to the rear projection screen. Thus, there were two mirror-image projections of the same stimulus visible on the screen. Each image could be changed in intensity by manipulating the rotatable plane polarizer or in position by manipulating the horizontal and vertical stimulus-deflector mirrors in each stimulus-deflector system. Details of this projection system can be found in report N14-0742-81C-001 entitled "The Effect of Interocular Contrast and Ocular

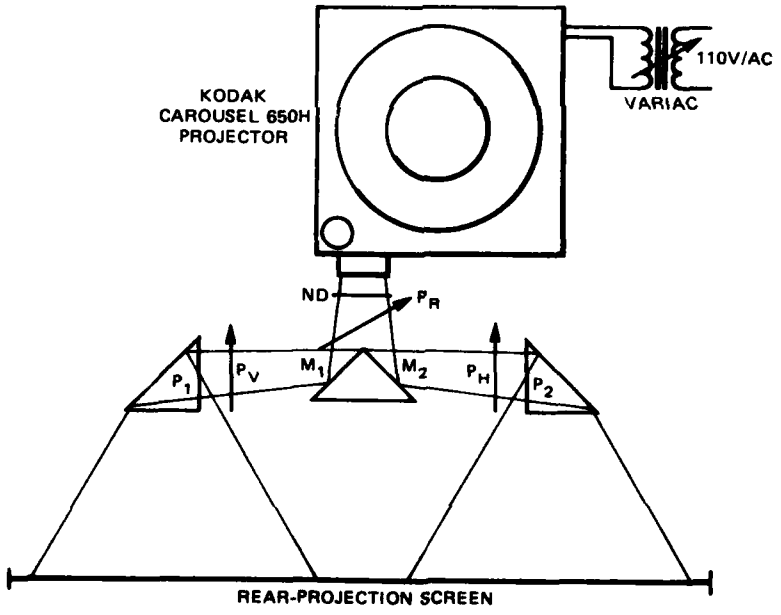

FIGURE 3 SCHEMATIC OF DISPLAY SYSTEM

ND, neutral density filter; P_R, rotatable plane polarizer; P_V, vertical plane polarizer; P_H, horizontal plane polarizer; M_1 and M_2, front surface mirrors; P_1 and P_2, prisms.

Dominance on the Perception of Motion-in-Depth in 3-D Displays," a technical report prepared for the Office of Naval Research in August 1981.

The computer-controlled, three-dimensional display system is positioned at right angles to the rear projection screen. To view this display system, a large front-surface mirror is positioned between the stimulus deflectors and the rear projection screen. This mirror is positioned close enough to the stimulus deflectors so that each of the observer's eyes sees only one of the Tektronix 602 display monitors.

Each monitor presents a 256 x 256 array of picture elements or "pixels." Each pixel may be presented at any one of 256 possible levels of intensity. The display beam scans the 256 x 256 image frame vertically at a rate of 100 frames per second. Scanning is controlled by a PDP-11/10 computer. This computer generates pattern parameters, controls scaling and rotation of the array, times the onset and offset of each display monitor, and provides data acquisition capabilities. The computer-controlled display system allows us to vary stimulus parameters along dimensions such as rotation and size that would be very difficult to produce with our rear-projection system.

Subject Response Apparatus--Because observers were fixed in position with dental impression bite-bars, they were unable to communicate their perceptions verbally. To facilitate communications, and to allow temporal comparison among physical stimulus events, physiological subject events, and perceptual subject events, observers operated a three-position switch to indicate changes in perceptual state. Where more than three states were to be specified, the subject operated a pair of three-position switches. Observer responses were recorded on a strip chart, in computer memory, or both.

Recording Apparatus--A variety of recording systems was used during the course of the study. The most commonly used was a four-channel Brush recorder with two event markers. This instrument can record output from the eyetracker as well as up to two channels of subject response. Usually, recordings of the type shown in Figure 4 were made. These consist of left and right horizontal eye-movement signals from the eyetracker, a vergence signal produced by differencing the left and right horizontal eye-movement signals and filtering the high-frequency components, a trace that shows the frequency and amplitude of stimulus motion, and an event marker that indicates whether the subject is perceiving the stimulus object moving laterally, ambiguously, or in depth. During the portions of this study in which data acquisition was via computer, subject responses were displayed off-line from computer memory. Raw and analyzed data were displayed on a Tektronix type 611 storage display unit and hard copies were obtainable on an Epson recorder.

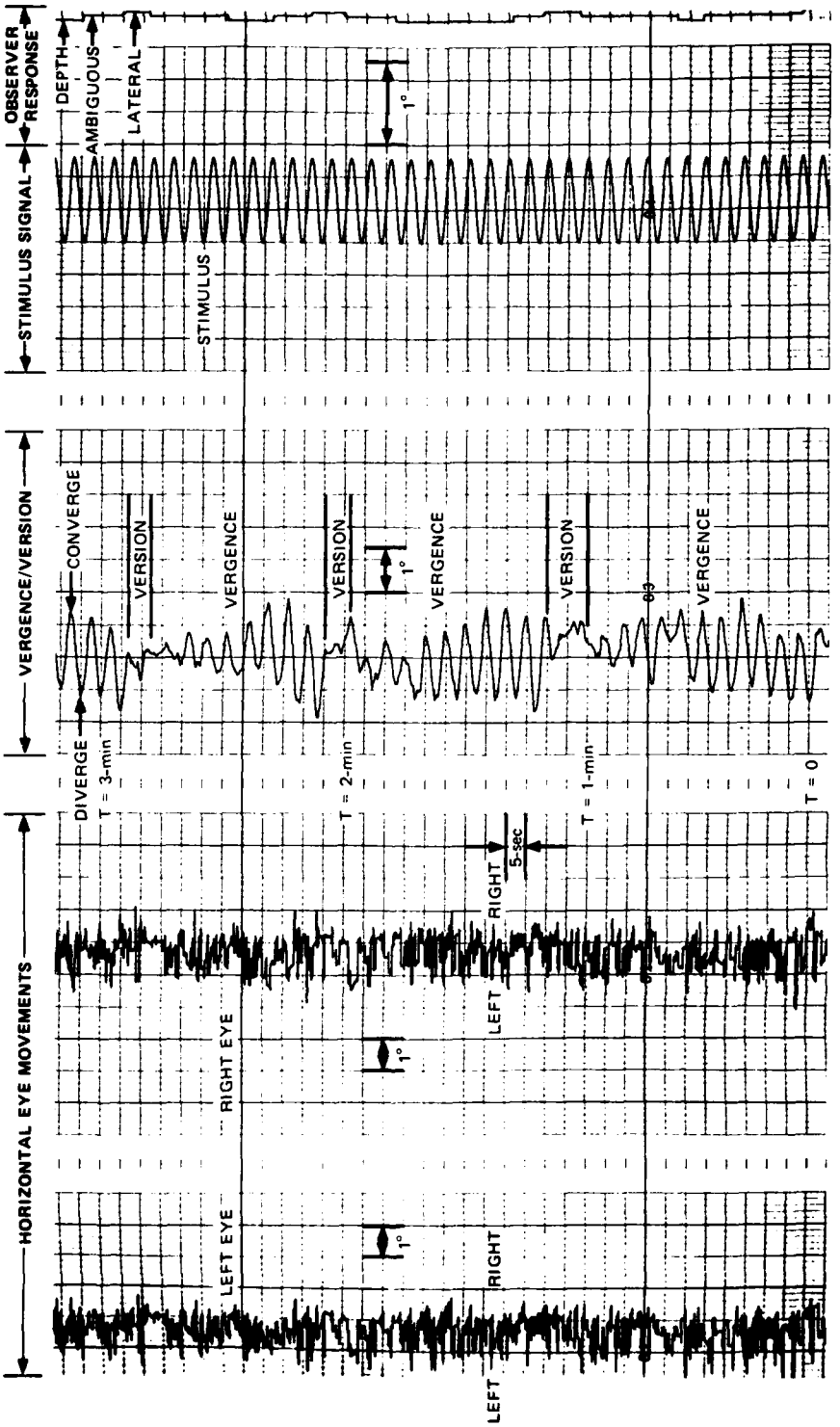

FIGURE 4 PHYSIOLOGICAL AND SUBJECTIVE MEASURES OF OBSERVER RESPONSES

Subjects

Fourteen subjects ranging in age from 18 to 42 years participated in this study. However, not all subjects participated in each experiment. During the preliminary phenomenological investigations involving stabilized images, and in the subsequent quantification of data obtained through the use of selected image stabilization, two well-trained observers, the author and Dr. Robert W. Hammon, served as subjects.

Not all subjects were emmetropic. To compensate for any spherical refractive errors, the investigator moved the focusing mechanism of the stimulus deflector until the subject indicated best visual acuity. When necessary, cylindrical lenses of appropriate power were positioned in the stimulus deflector at a plane conjugate to the subject's pupil and oriented to cancel astigmatic errors. Ocular dominance was tested with a pin-hole sighting procedure.

III RESULTS

Both qualitative and quantitative measures of perceptual response were used in the course of the study. In either case the goal of any given experiment was a perceptual change occurring as a result of manipulating stimulus variables. Two techniques were used to manipulate the stimulus variables: a selectively stabilized image technique and an unstabilized motion-in-depth technique. The selectivity stabilized image technique produced our phenomenological observations, while the motion-in-depth technique produced quantitative data. A combination of both techniques was used to quantify the phenomenology we observed early in this investigation.

Selectively Stabilized Images

The selectively stabilized image technique uses the eyetracker to measure a subject's horizontal and vertical eye rotations. These signals are fed through an amplifier to the horizontal and vertical mirrors of the stimulus deflector system, respectively. When the amplifier gains are set accurately, the image motion produced by the deflection mirrors exactly cancels the retinal image motion produced by the subject's eye movements. As a result, the image is precisely stabilized on the subject's retina. Up to this point, the technique is conceptually similar to other stabilized image techniques. However, a feature of the stimulus deflector system allows unstabilized stimuli to be presented to the subject at the same time other stimuli are stabilized. Unstabilized stimuli are introduced at a plane conjugate to the retina identified as the unstabilized image plane in Figure 2. Unstabilized stimuli in the form of edges, apertures, or fixation points were used as required to present the subject with isolated luminance or chrominance edges or stationary planes or points of reference that do not disappear due to image stabilization.

Our earliest observations involved the use of the selectivity stabilized technique to evaluate the effect of loss of luminance edge information or chrominance edge information upon form and depth perception. In these experiments, subjects viewed a field bounded on either side by unstabilized edges, usually black, vertical occluders. Stimuli presented in the field seen between the occluders were stabilized to disappearance.

This series of experiments indicated to us the profound effect that edge information has on form perception and induced us to explore the role of edge information in stereopsis. To cite a few examples of the effects of edges on perception, we were able to alter the perception of the same physical stimulus to that of either a uniform green field or a

uniform red field simply by positioning unstabilized edges differently in the field. More specifically, when we presented subjects with a red disk surrounded by a contiguous green annulus and stabilized the image of the boundary between the red disk and green annulus, we could make the field appear entirely green by placing an unstabilized black surround so that its edge fell entirely within the green annulus. We could also make the same stimulus appear completely red by placing in the center of the red disk a black unstabilized disk whose edges fell entirely within the red area. Both of these are examples of the filling-in phenomenon that occurs under normal viewing conditions when part of an image is suppressed.

As another example, when we presented subjects with a stabilized image consisting of two chromatic stripes, a green stripe on the left and a red stripe on the right, whose common boundary was stabilized and whose outer edges were covered by unstabilized black occluders, the field appeared filled with a color that has been thought to be theoretically impossible. The color was described by many subjects as reddish-green. Once again, the percept is consistent with the available edge information in the visual stimulus. On the left side, the subject sees a distinct black-green edge and on the right side, a distinct red-black edge, but there is no perceptible boundary between the red and the green stripe. The chromatic information available at each edge is filled in across the field to the next perceptible edge, resulting in the perception of this forbidden color.

The chromatic results presented above, as well as achromatic results of experiments in which luminance edges were stabilized to disappearance, indicated to us that edges are extremely important in determining the form and position of stimulus objects. Furthermore, our results indicate that luminance and chrominance edge information are handled somewhat differently by the visual system. Chromatic edges without any luminance component disappear much more rapidly than luminance edges and seem to be incapable of supporting the perception of form. These results prompted us to examine the effect of the same variables on depth perception. We questioned whether the visual system might be capable of using the edge information available to both eyes to determine the three-dimensional position of a stimulus object even when form perception of that object had been eliminated in one eye by image stabilization.

Preliminary phenomenological investigations of the perception of motion-in-depth during the disappearance of one of a pair of binocular images due to image stabilization suggested that form perception may cease due to image stabilization but depth perception does not. In that series of experiments, subjects viewed the same stimulus object through each stimulus deflector. Each eye viewed, for example, a black bar on a white background bordered by unstabilized black occluders. Before stabilizing either image of the black bar, when the image of the black bar was oscillated sinusoidally back and forth in one eye (with a frequency of approximately 0.2 Hz and and amplitude of 1^{o} peak-to-peak), subjects reported seeing the fused image of a single black bar that appeared to

move in depth along a diagonal path. When the image of the black bar was stabilized on the subject's other retina and its companion image on the first retina was oscillated back and forth, as before, subjects still reported seeing the bar moving in depth along a diagonal path. This observation indicates that the visual system monitors the edges of both retinal images even though the edges of the stabilized retinal image had disappeared.

When we performed the chromatic analog of the preceding experiment, by presenting to the subject an isoluminant red bar on a green field instead of a black bar on a white field, the perception of motion-in-depth under the unstabilized condition was marginal, and under the monocularly stabilized condition, completely absent. Thus it seemed to us that chromatic edge information was not used by the visual system for generating the perception of motion-in-depth.

We have subsequently quantified our observation of the persistence of the percept of motion-in-depth during disappearance of one of a pair of binocular images. We did this by measuring the spatial contrast sensitivity function first with both monocular images visible and then with one of the images stabilized to disappearance.

In the experimental paradigm that we used, each eye viewed a vertical sinewave grating of the same spatial frequency filling a circular aperture of about 6^{o} angular subtense. One grating was presented at a constant modulation of 25 percent, while the modulation of the other could be varied by the experimenter. Superimposed on the image seen by each eye was a fixation target that was stationary in the field of view. During each experimental run, one of ten spatial frequencies ranging from 0.4 to 9.2 cycles per degree was presented. The image of the variable-modulation grating was translated left and right with a triangular waveform having a frequency of 1/2 Hz and amplitude of 1^{o} peak to peak.

When the contrast of the moving grating was high enough to support stereopsis, the resulting perception was of a grating moving in depth relative to the fixation point. When the contrast of the moving grating was too low to support stereopsis, the subject saw this grating moving laterally. When the contrast was very low, the subject saw only the stationary grating.

Each trial within a run was initiated by presenting the subject with a moving grating at a particular modulation. The subject's task was to decide which of the following categories best described the motion of the grating: motion-in-depth only, mostly depth-motion, ambiguous motion, mostly lateral motion, and lateral motion only. Each run consisted of approximately 25 trials at a given spatial frequency.

The threshold for the detection of motion-in-depth was defined as the mean of the modulation values of the variable grating resulting in the subject's response of either motion-in-depth only or mostly motion-in-depth. Likewise, the threshold for the perception of lateral motion

was defined as the mean of the modulation values of the variable grating that resulted in the subject's response of lateral motion only or mostly lateral motion. These threshold values were plotted as a function of spatial frequency to produce motion-in-depth and lateral-motion contrast sensitivity functions. Figure 5(a) shows the threshold for the perception of motion-in-depth and for the perception of lateral motion under unstabilized conditions at each of the ten spatial frequencies.

Thresholds for perceiving motion-in-depth and lateral motion, with one image stabilized, were obtained by the same procedure. These thresholds are plotted in Figure 5(b) as a function of the spatial frequency of the grating. They reveal the spatial contrast sensitivity function of the motion-in-depth perception mechanism in the absence of form perception in one eye. As one might expect from the description of the observer's task, the data are somewhat noisier than the unstabilized data. Nonetheless, these data show that the effect we observed some time ago, namely that perception of motion-in-depth is not eliminated by stabilized disappearance in one eye, is both real and quantifiable. The most striking feature of these curves is that the modulation required for the perception of motion-in-depth is lower at most of the spatial frequencies tested when the grating is stabilized to disappearance in one eye, than when it is visible to both eyes. This implies that form perception may inhibit the perception of motion-in-depth, at least in the range of 1 to 5 cycles per degree.

Because the perception of motion-in-depth persisted during stabilization of one of a pair of binocular images to disappearance, we questioned whether it might also be possible for depth perception to persist in the absence of form perception in both eyes. To answer this question, we presented the subject with a binocular display each of whose images consisted of

- A vertical black bar on a white background.
- Unstabilized black occluders forming the left and right boundaries of the background.
- An unstabilized fixation point near the center of the field.

(Initial observations with this paradigm indicated that the fixation points were essential for preventing vergence movements during stabilization of the black-bar stimuli.) The subject positioned the left- and right-eye images of the occluders and of the fixation targets so that they appeared fused. Thus, the subject perceived a single fixation point centered within a single aperture. Within this aperture, the subject viewed the image of the black bar on the white background. In each eye, the retinal image of the black bar was displaced nasally, resulting in the perception of a fused black bar that appeared to lie in a plane behind the fixation point--i.e., at a greater distance from the subject than the fixation point. This is shown in Figure 6. When the image of the black bar was stabilized to disappearance in both eyes, the subject

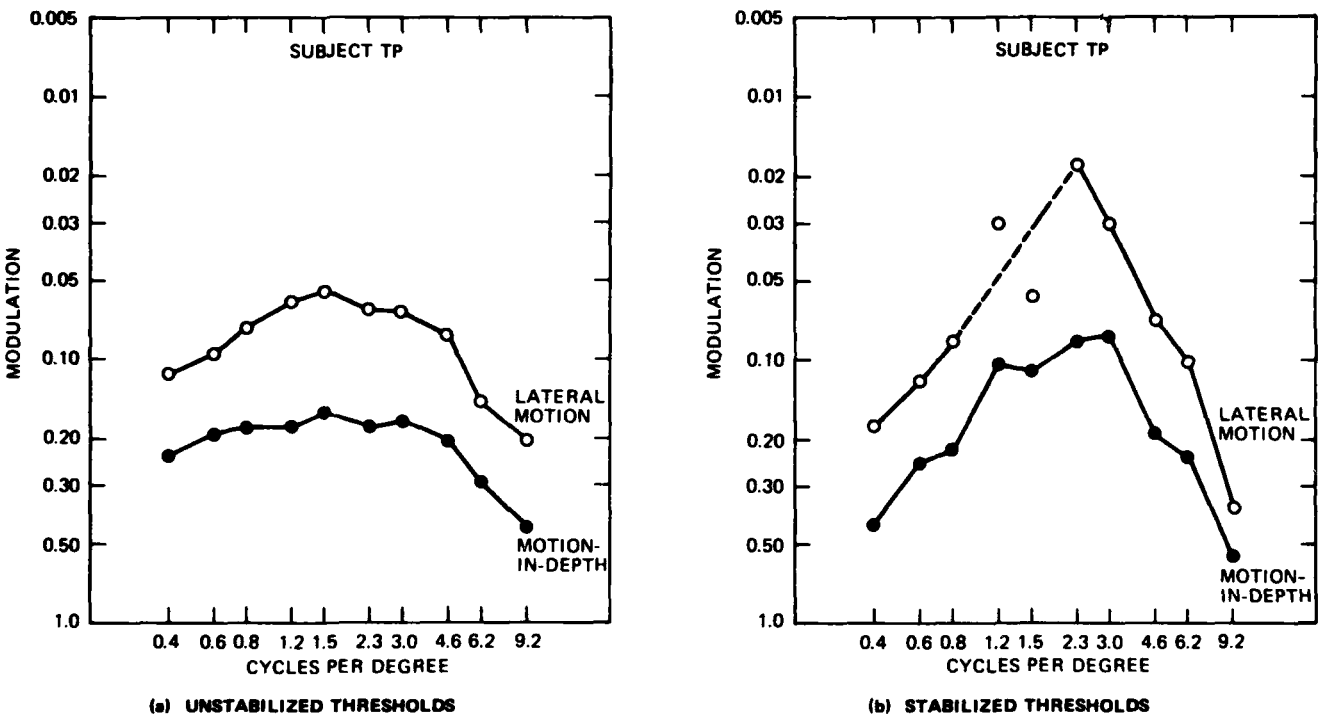

FIGURE 5 COMPARISON OF STABILIZED AND UNSTABILIZED THRESHOLDS

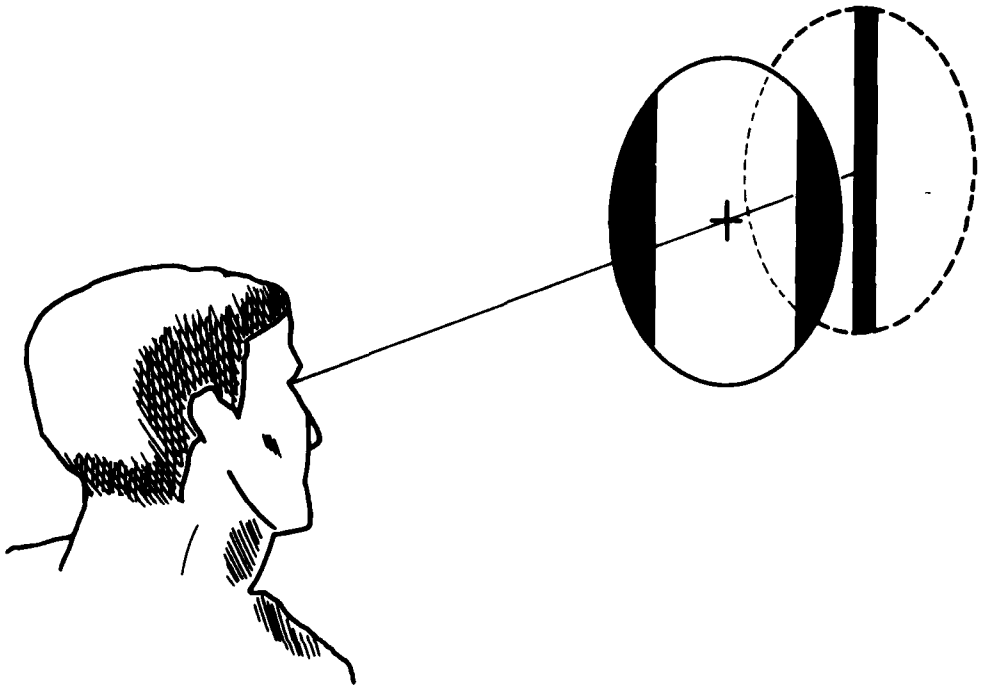

FIGURE 6 PERCEIVED IMAGE PLANES BEFORE DISAPPEARANCE OF THE STABILIZED IMAGES

The observer views stereoscopic images of a black bar that appears to be positioned behind the fixation point (cross). Two depth planes are produced: the plane of fixation and the more distant plane containing the black bar.

reported the perception of a plane corresponding the plane that contained the now-invisible black bar. The subject's spatial perception of the stimulus array after disappearance of the bar is shown in Figure 7.

These observations suggested to us that the human stereo mechanism might be capable of using information present in the retinal image that does not reach perceptual awareness. To test this observation, we modified our apparatus so that it included an unstabilized image of a vertical black bar that could be used as a pointer to indicate the depth plane of other stimuli seen in the field. The range of excursion of the pointer encompassed both the depth plane of the fixation target and of the black bar.

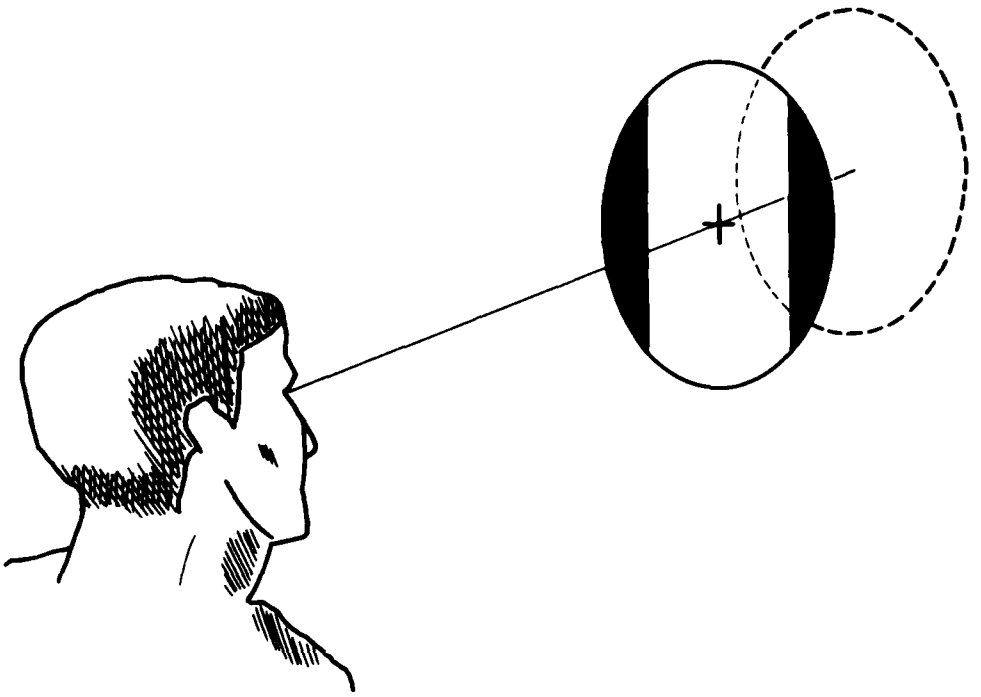

FIGURE 7 PERCEIVED IMAGE PLANES AFTER DISAPPEARANCE OF THE STABILIZED IMAGES

The image of the black bar is stabilized on each retina and therefore the black bar disappears. However, the depth plane that that the bar occupies is still perceived as a uniform field at some distance behind the fixation point.

In unstabilized trials, the experimenter moved the pointer until the subject indicated that it was the same distance from him as the fixation point. The experimenter then moved the pointer until the subject indicated that it was at the same distance from him as the black bar. Ten trials of each type were conducted and the mean and standard deviation of the perceived depth plane of the fixation target and the black bar were calculated. The same procedure was used in stabilized experiments during which the image of the black bar had disappeared. Under these conditions the subject's task was to state when the pointer was at the same distance from him as the fixation target, and then to indicate when the pointer was at the same distance from him as the uniform field

containing the invisible black bar. Ten trials of each type were conducted and the means and standard deviations calculated for the location of the fixation point and the uniform field.

The data shown in Figure 8 indicate that under unstabilized conditions, the black bar appears to be approximately 20 to 25 cm behind the fixation point. Under stabilized conditions, the uniform field containing the invisible black bar also appears to be 20 to 25 cm behind the fixation target. These data support the assumption that the stereo mechanism continues to generate the perception of depth when form perception has been eliminated in both eyes due to retinal image stabilization.

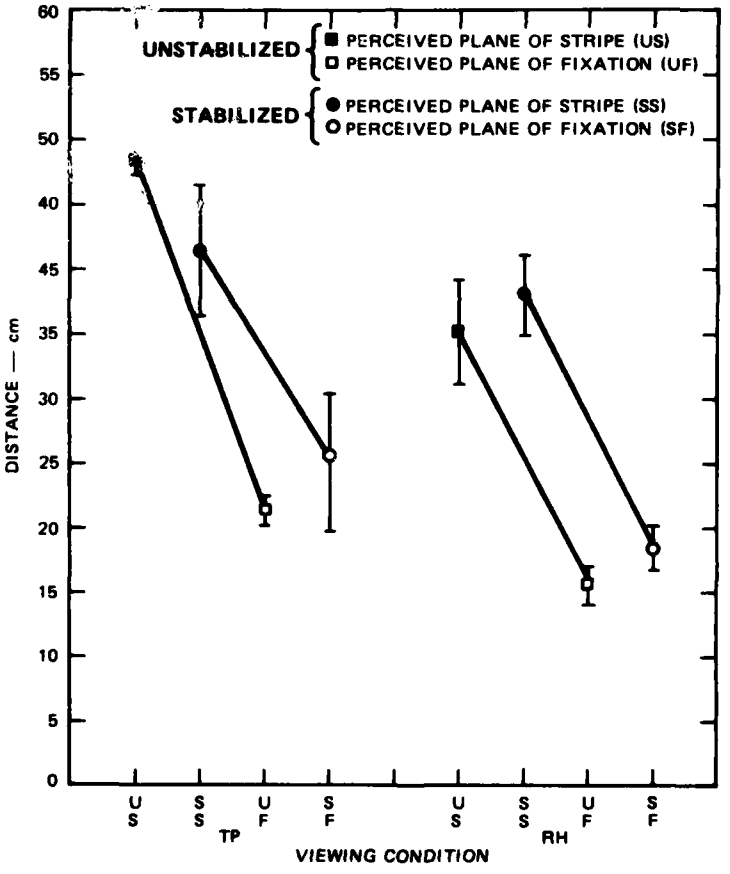

FIGURE 8 PERCEIVED DISTANCE TO FIXATION POINT AND PLANE OF STRIPE

As previously alluded to, the fixation target was necessary in the binocular stabilization studies to minimize vergence movements during disappearance of the binocular stimuli. Our monocular stabilization studies demonstrated that during periods of image disappearance, movements of the eye in which the image was stabilized showed idiosyncratic drift patterns. In fact, during monocular stabilization, it was usually possible for the experimenter to tell when the stabilized image had disappeared by characteristic changes in the subject's eye movements. However, because the subject's other eye continued to view an unstabilized (and therefore visible) image, the resultant eye-movement patterns appeared normal. Furthermore, these normal eye movements in the seeing eye tended to align the gaze angle of the subject's nonseeing eye. When we stabilized the images in both eyes, the previously available anchoring stimulus was eliminated. Under these conditions, before disappearance of the binocularly stabilized image, subjects reported seeing the fused black binocular stimulus moving indepth. In fact, this perceived motion-in-depth was frequently very compelling and very rapid. An analysis of the eye-movement records obtained during binocular image stabilization without fixation targets showed that subjects were making large-amplitude vergence movements during periods when they reported the perception of motion-in-depth of the stimulus object. Furthermore, when they reported the approach of the stimulus object, their eye-movements records indicated that they were making convergent movements.

With our image-stabilization technique it was easy to vary the signal gain between the eyetracker and the stimulus deflector. Because the gain controls the amplitude of the retinal image motion for a given eye movement, it also affects dynamic retinal disparity under binocular viewing conditions. When the gain is zero, retinal image motion and disparity changes are the same as during normal unstabilized vision; when the gain is unity, the image is stabilized, so no disparity changes occur with eye movements. Thus, the foregoing results indicate that when retinal disparity changes are eliminated by stabilization of both retinal images, a subject's vergence system drives his stereo mechanism, producing the perception of motion-in-depth. Because we also have control over absolute retinal position of stimuli, it was possible to generate stimuli of any static retinal disparity. Furthermore, with stabilization, that disparity could not be changed by a subject's eye movements. By using this capability we explored the interaction between static retinal disparity and vergence. We found that when the binocular stimuli were imaged without static retinal disparity--that is, when each fovea was positioned in the same location relative to its image--the effect of vergence eye movements on the perception of motion-in-depth was minimized. When static retinal disparity was increased, either in the crossed or the uncrossed mode, a given vergence eye movement resulted in a much stronger percept of motion-in-depth of the fused binocular stimulus.

In a related experiment, the gain between the eyetracker and stimulus deflector was set above unity. With gain above unity, the change in disparity produced by a given eye movement is <u>opposite</u> to that which occurs with normal eye movements. Consequently, convergent eye

movements produce dynamic retinal disparities that are consistent with those that are normally produced by divergent eye movements. We found that a well-trained subject is capable of setting the gain between the eyetracker and stimulus deflector such that the reverse-polarity-dynamic-retinal-disparity signals exactly cancel the vergence inputs to the stereo mechanism. Under these conditions the subject could make vergence eye movements without experiencing any motion-in-depth. On several occasions, when the subject had increased the gain slightly above the setting that canceled the vergence and disparity inputs to stereopsis, convergence eye movements resulted in the perception of the fused object receding rather than advancing. These experiments seem to suggest that retinal disparity and vergence may be evaluated not only individually but also symbiotically.

Motion-In-Depth

Our motion-in-depth studies involved the use of stereograms presented either on the rear projection screen or on the computer-controlled three-dimensional display system. With both stimulus configurations, subjects were positioned with respect to the eyetracker by a dental impression bite-bar and viewed the stimuli through the stimulus deflectors. In the experiments presented here, the stimulus deflectors were used to move the retinal images, but not to stabilize them.

In the first series of experiments, we evaluated the luminance level, contrast level, and interocular contrast of the stereo pairs on the rear projection system. The stereo pairs were produced by inserting a slide into the projection system shown in Figure 3. With either eye, subjects saw an image of the slide centered in a 10^{o} circular field. The pattern seen by each eye was a light square subtending approximately 4^{o} on a side viewed against a dark background. The contrast between the square and its background was maintained at one of several values: 37, 49, 67, 83, or 96 percent. (These contrast percentages are reported nominally as 20, 40, 60, 80, and 100, but are plotted in the accompanying figures at ordinates consistent with their actual percent contrast values.) The target squares were presented at one of two mean luminance levels: 1.5 or 3.0 foot lamberts (fL). Interocular contrast--that is, the difference in luminance between the two stereo images--was controlled by the variable polarizer shown in Figure 3.

The image of the target seen by either eye was moved back and forth laterally in the field of view by oscillating the horizontal stimulus deflector mirror with a frequency of 0.2 Hz and a peak-to-peak amplitude of 1^{o}. The left and right horizontal stimulus-deflector mirrors moved in antiphase, so that when conditions favored stereopsis, the subject reported seeing a single fused stimulus moving in-depth along the midline.

In this study both objective and subjective measures of stereopsis were obtained. Objective measures consisted of binocular, horizontal eye-movement records and a vergence signal synthesized by differencing

them. Subjective measures of the motion of the stimulus object were obtained by requiring the subject to move a three-position switch to indicate whether the stimulus was seen moving only in-depth, ambiguously, or only laterally. These measures were shown in Figure 4 along with a trace indicating the amplitude and frequency of the horizontal stimulus-deflector mirrors, identified as the stimulus signal.

In each experimental session, a slide containing a stimulus at one of the contrast levels was placed in the projector, and the variable polarizer was set at a position consistent with the type of trial to be conducted. When the variable polarizer was set at the 45° position, the interocular contrast was near unity and the subject saw the stimulus moving only indepth. When the variable polarizer was set near 0 or 90°, the interocular contrast ratio was high, resulting in the subject's perception of lateral motion only of the stimulus. The end point of each trial occurred when the subject indicated that the perceived motion of the stimulus had changed state, either from lateral only to depth only or vice versa. Within each type of trial, two symmetrical series were run, one that increased the luminance of the image seen by the left eye and another that increased the luminance seen by the right eye. Ten trials were run in each of the symmetric series for a total of 20 trials per experimental session.

The angular position of the plane polarizer at which the subject saw a complete change of state was converted to an interocular contrast ratio. These data for the interocular contrast ratios at which the perception changed from motion-in-depth only to ambiguous to lateral motion only, when the stimulus had a mean luminance of 1.5 fL, is plotted in Figure 9 as a function of the slide contrast for trained observers and for naive observers. Notice that trained observers continue to see unambiguous motion-in-depth at interocular contrast ratios where naive observers see only ambiguous motion.

Similar data were analyzed for the effect of ocular dominance. Figure 10 shows an example of the difference in effect depending upon whether the luminance was reduced in a subject's dominant or nondominant eye. Both ocular dominance and training were found to affect the interocular contrast ratios at which an observer could maintain the perception of motion-in-depth when viewing a three-dimensional display.

Following the evaluation of nominal stimulus contrast, stimulus luminance, and interocular contrast, we evaluated the effect of vertical registration of the two binocular stimuli on the perception of motion-in-depth. Each stimulus consisted of a light square subtending 4° on a side with a luminance of either 1.5 or 0.75 fL seen against a darker background. The contrast between the square and its background was nominally either 20, 60, or 100 percent. As in the previous experiment, horizontal stimulus motion was produced by driving the horizontal stimulus-deflection mirrors in antiphase with a sinusoidal signal of 1° peak-to-peak at a frequency of 0.2 Hz. In this experiment, the vertical deflection mirrors were used to vary the vertical alignment of the two stereo images. As the two images were misaligned vertically, the

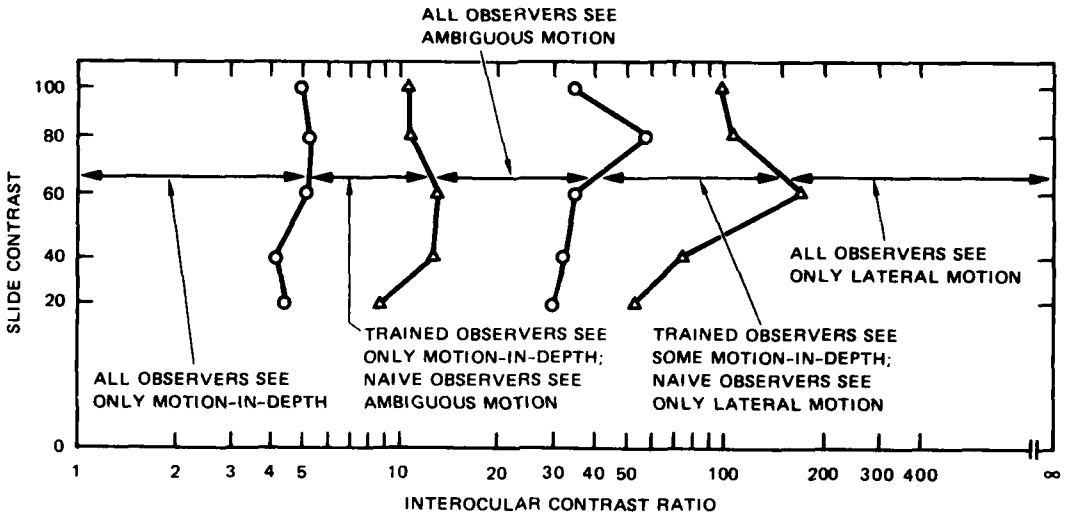

FIGURE 9 TRANSITION INTEROCULAR CONTRAST RATIOS OF TRAINED AND NAIVE OBSERVERS FOR THE PERCEPTION OF MOTION-IN-DEPTH, AMBIGUOUS MOTION, AND LATERAL MOTION OF A 1.5-fL STIMULUS

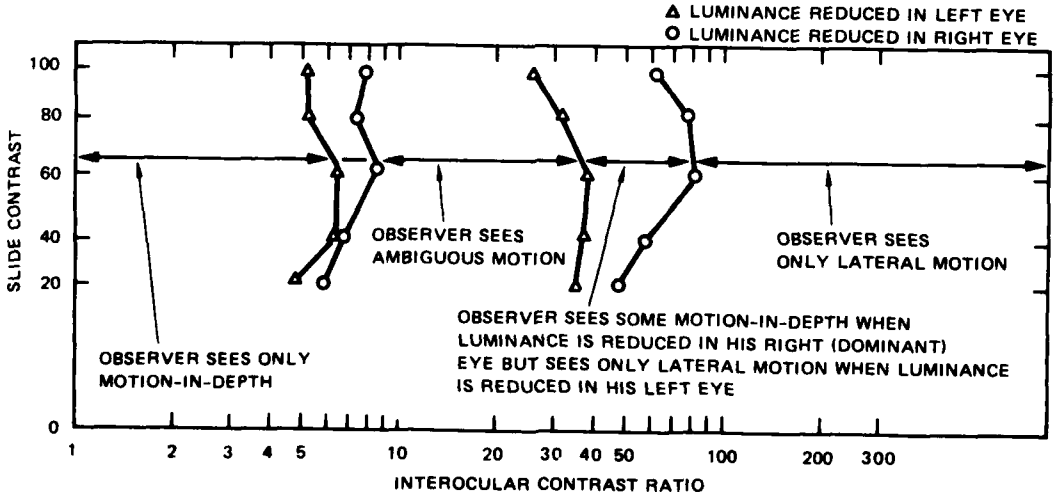

FIGURE 10 TRANSITION INTEROCULAR CONTRAST RATIOS OF THE DOMINANT AND NONDOMINANT EYES OF A RIGHT-EYE-DOMINANT OBSERVER FOR THE PERCEPTION OF MOTION-IN-DEPTH, AMBIGUOUS MOTION, AND LATERAL MOTION OF A 1.5-fL STIMULUS

subject was to report the perceived motion of the stimulus (lateral, ambiguous, or indepth) as well as the state of fusion of the two stimuli (completely fused, partially fused, not fused.) The experimenter recorded the amplitude of the dc signal to the vertical stimulus-deflector mirror that resulted in each of the response states. Because either image could be above or below the other, data are plotted as the mean of the absolute value of the number of degrees of misalignment between the two stimuli within which the subject saw the stimulus moving in a particular direction (indepth, ambiguously, or laterally).

Figure 11 shows data obtained from one of our subjects. Averaging across subjects, we can generalize that the images remained fused and the subjects saw motion-in-depth exclusively when the vertical misalignment of the two images was $< \pm 1^{o}$. When the vertical misalignment exceeded $\pm$ 1.5 to 2^{o}, subjects tended to see the stimulus moving ambiguously. When the vertical misalignment was between 2 and 4^{o}, subjects reported diplopia and exclusively lateral motion of the stimuli. These observations persisted across the dimension of stimulus luminance and stimulus contrast.

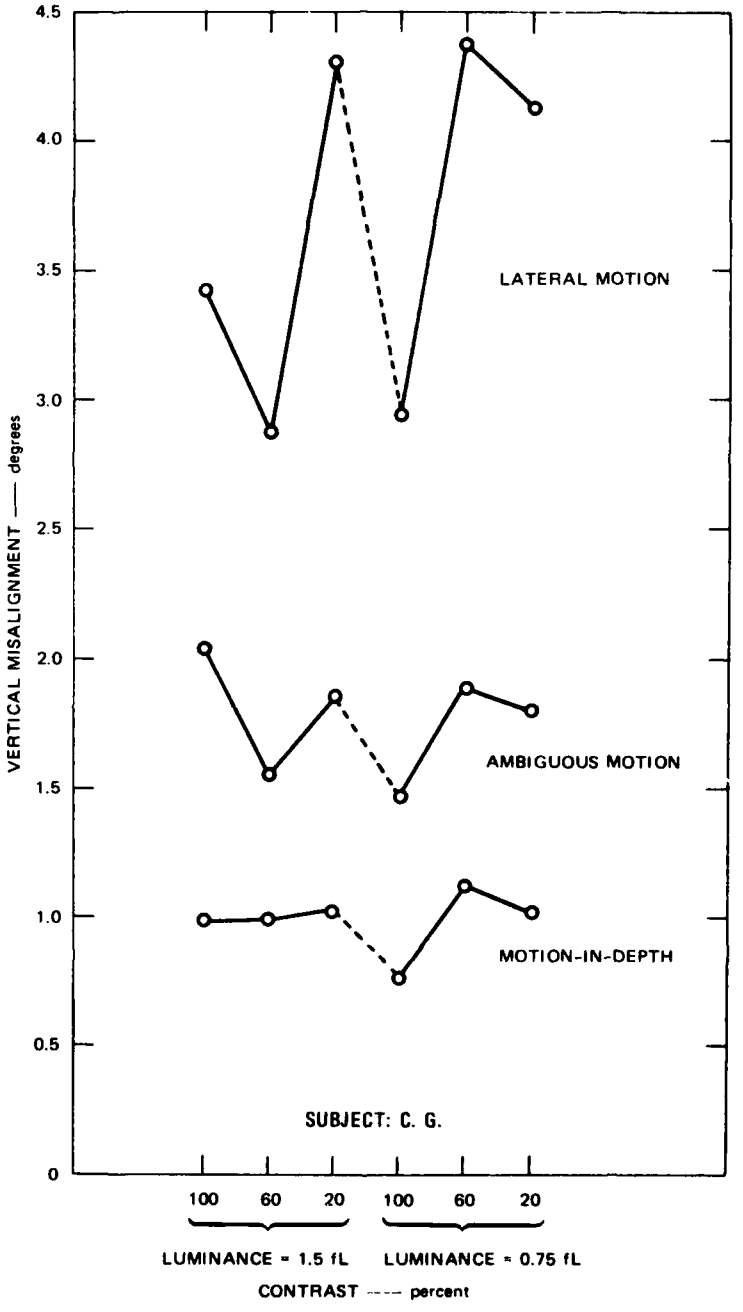

FIGURE 11 VERTICAL MISALIGNMENT OF BINOCULAR IMAGES RESULTING IN THE PERCEPTION OF MOTION-IN-DEPTH, AMBIGUOUS MOTION, AND LATERAL MOTION

IV DISCUSSION

The results of this study, including those obtained with the selectively stabilized image technique and the motion-in-depth technique, provide some basic understanding of the effect of various stimulus parameters upon the perception of depth in three-dimensional display systems. Although the initial emphasis of the investigation was not specifically to elucidate the effects of edges displayed in a three-dimensional system, discussion of the results may be couched in that context. The discussion will focus upon the manner in which edges and their degradation affect the perception of form, depth, and motion-in-depth in three-dimensional displays.

The experiments reported above, which examine the persistence of the perception of motion-in-depth during monocular image disappearance, suggest that the human stereopsis mechanism is sensitive to the edges present in retinal images even if those edges fail to reach perceptual awareness. To generate the perception of motion-in-depth in the absence of any monocular motion-in-depth cues, it is necessary for the human stereopsis mechanism to compare the location and changes in location of corresponding edges in both retinal images. The results reported here suggest that this capability is not dependent upon the binocular perception of form produced by these same edges. Furthermore, there is evidence presented in Figure 5 that the monocular perception of form may even inhibit the perception of motion-in-depth.

The foregoing discussion of form perception and motion-in-depth perception should be prefaced by the statement that the discussion pertains only to luminance edges. Our study of the effect of isoluminant chromatic edges on the perception of motion-in-depth during disappearance of a stabilized image in one eye indicates that the human stereopsis mechanism is insensitive to purely chromatic edges in the retinal image. That is, edges that consist of changes only in chromaticity but not in luminance do not appear to support stereopsis. In fact, when images consisting of an alternating series of chromatic edges and luminous edges are moved laterally on one of the subject's retinas, the binocularly perceived pattern is the same as the stimulus pattern but its perceived motion is ambiguous, probably due to conflicting inputs to the stereopsis and form-perception mechanisms.

The experiments reported above that involve stabilization of both images of the stereogram suggest that the stereopsis mechanism does not require form perception in either eye to generate the static perception of depth. When corresponding luminance edges are presented on both retinas, the stereopsis mechanism can compared the location of these corresponding edges relative to other features in the retinal images irrespective of whether these corresponding edges are available to form

perception. Once again, the dichotomy of luminance edges and chromatic edges is apparent in static depth perception. Experiments with isoluminant chromatic stimuli suggest that the mechanism responsible for static depth perception is sensitive only to the luminance edges present in the retinal images.

Experiments in which all foveal and parafoveal stimuli were stabilized to disappearance in both eyes revealed that vergence movements per se were capable of producing a compelling percept of motion-in-depth. Because the images were stabilized, this percept occurred in the complete absence of changes in retinal disparity normally occurring as a consequence of eye movements. It seems, then, that inputs to stereopsis from eye movements are capable of driving that mechanism even in the absence of changes in the relative position of edges in both retinal images. Furthermore, when the corresponding retinal images of an edge are stabilized with some static disparity, either crossed or uncrossed, the input from the vergence mechanism to stereopsis is enhanced. This can be interpreted to mean that the position of binocularly represented edges relative to the fovea is important in determining both the static perception of depth and the magnitude of the perception of motion-in-depth produced by vergence.

The magnitude of the effect of vergence input and of dynamic retinal disparity input to stereopsis can be measured separately by rendering these inputs antagonistic. Our preliminary experiments in this area have demonstrated the feasibility of such a procedure by showing on a phenomenological level that the magnitude of reversed-polarity dynamic retinal disparity inputs can be adjusted to exactly cancel inputs from vergence.

Further systematic studies of the effects of luminance edges on the perception of motion-in-depth revealed the dependence of the motion-in-depth mechanism not only upon the luminance and contrast of edges in the retinal image, but also upon the difference in luminance and contrast between the two retinal images. This latter quantity we called interocular contrast. The studies of interocular contrast presented here suggest that the perception of motion-in-depth in stereo displays is partially dependent upon such subjective factors as the ocular dominance of the observer and the amount of experience the observer has had with three-dimensional displays.

Our studies of physical parameters, such as vertical and rotational image misalignment, suggest that the correspondence of edges in the two retinal images is determined largely by a recognition of objects by the form-perception mechanism. When the images of objects are displaced in particular ways, the efficacy of the edges of these objects in producing the perception of motion-in-depth is diminished. The vertical image registration studies suggest that loss of the perception of motion-in-depth parallels the loss of fusion of the binocular images but is not

identical to it. Furthermore, fusion may depend either upon the absolute vertical angular displacement of horizontal edges that define objects or upon the percentage of the area of the object displaced vertically on the two retinas.

In conclusion, the studies reported here suggest that edges are critical to the production of static depth and motion-in-depth, but that the description of a retinal image edge provided by the form-perception mechanism may vary from that perceived by the depth-perception mechanism. When we understand more fully what constitutes an edge for the depth-perception mechanism, we may be able to modify three-dimensional display systems to take advantage of the differences in the way the form-perception and depth-perception mechanisms treat the same retinal image information.

V DISSEMINATION OF INFORMATION

The principal investigator attended several conferences where he reported the findings of this study. In October 1979, he co-authored a paper with Dr. Hewitt D. Crane entitled "Selectively Stabilized Retinal Images" that was presented at the European Conference on Visual Perception in Noordwijkerhout, The Netherlands. This paper reported the essence of the selectively stabilized image technique and outlined some of the early phenomenological observations made with it.

In January 1980, the principal investigator attended the Oculo-Motor Symposium 80 at Cal Tech in Pasadena where he presented a paper entitled "Selectivity Stabilized Images" co-authored by Dr. Hewitt D. Crane. This report described the selective image stabilization technique and reported our observations while using it.

A report co-authored by the principal investigator and Dr. Hewitt D. Crane entitled "Stereopsis Without Binocular Perception or Retinal Disparity" was presented at the Topical Meeting on Recent Advances in Vision sponsored by the Optical Society of America in Sarasota, Florida during April 1980. This report concentrated on the effects of image stabilization on binocular vision and stereopsis.

In April 1981, the principal investigator in collaboration with Dr. Hewitt D. Crane presented a paper entitled "Depth Perception with Selectively Stabilized Images" at the Spring Meeting of The Association for Research in Vision and Ophthalmology in Sarasota, Florida. This report was the first quantitative description of the persistence of perceiving motion-in-depth during stabilization of one of a pair of binocular images.

A technical report entitled "The Effect of Interocular Contrast and Ocular Dominance on the Perception of Motion-in-Depth in 3-D Displays" was written in 1981 by the principal investigator and Dr. Robert W. Hammon. This technical report documented the effects of changes in the mean luminance level and interocular contrast on the unambiguous perception of motion-in-depth in three-dimensional display systems, as well as describing changes in the perception of motion-in-depth attributable to the ocular dominance of observers. This report has been submitted to the Catalogue of Selected Documents in Psychology.

During October 1981, the principal investigator attended a workshop on modeling control of eye movements at Carnegie-Mellon University. This workshop was sponsored by the U.S. Naval Air Systems Command/Naval

Training Equipment Center. The principal investigator presented a paper entitled "Stereopsis Without Binocular Perception or Retinal Disparity," which updated his findings on the effect of partial or complete image stabilization on stereopsis.

In January 1982, the author will present a paper entitled "Stereopsis Has the 'Edge' In 3-D Displays" to be read at a meeting jointly sponsored by the National Research Council's Committee on Human Factors and the Naval Air Systems Command. This paper will summarize the results of this study, and will integrate information gained through stabilized and unstabilized techniques.

A manuscript tentatively entitled "Separation of Form and Depth Perception by Retinal Image Stabilization" is in preparation. When completed, it will be submitted to Science. A second manuscript based upon the Technical Report mentioned above is in preparation for submission to Vision Research.

Appendix A

ACCURATE THREE-DIMENSIONAL EYETRACKER

Reprinted from Applied Optics, Vol. 17, No. 5, pp. 691-705 (1 March 1978)

Reprinted from APPLIED OPTICS, Vol. 17, page 691, March 1, 1978

Accurate three-dimensional eyetracker

H. D. Crane and C. M. Steele

A combined optometer and eyetracking instrument has been developed to measure both the dynamic refractive power and the direction of gaze of the same eye. In effect, this instrument measures, as a function of time, the point in 3-D space on which the eye is fixated. Nothing is attached to the subject (patient), who is easily aligned in the device. The measuring wavelength is in the near ir and is invisible. The usable field of the instrument is greater than 20°; the horizontal and vertical directions of gaze are measured with a noise level and repeatability of about 1 min of arc. The range of the optometer is approximately −4 to +12 diopters; refractive power is measured to about 0.1 diopter. Two instruments may be aligned side by side for tracking both eyes simultaneously. Three-dimensional monocular and binocular eye movement records are shown.

I. Introduction

The instrument described in this article evolved from a series of experiments on the mechanisms of visual accommodation. Early in our accommodation studies, it became apparent that merely measuring the refractive power of the eye was not sufficient. We were also interested in isolating small retinal areas (to map sensitivity to blur over different regions of the retina) and in measuring the interaction between eye movements and the accommodation system. For these studies, the two measurement instruments described in this paper were developed to function simultaneously on the same eye: an optometer[1] to measure the refractive power of the eye and a double-Purkinje-image eyetracker[2] to measure the direction of the visual axis, both continuously. Experimental paradigms are much more restricted if accommodation measurements are limited to one eye, while eye-movement measurements are performed on the other eye.

This newly developed instrument system measures the point in three-dimensional (3-D) space on which the eye is fixated. The instrument can thus be thought of as a 3-D eyetracker. The direction of gaze is measured with a noise level and repeatability of about 1 min of arc rms. Refractive power is measured with a noise level of about 0.1 diopter.

The authors are with Stanford Research Institute, Menlo Park, California 94025.

Received 2 July 1977
0003-6935/78/0301-0691$0.50/0.

The fundamental operating principle of each instrument is discussed separately, followed by a description of the combined instrument.

II. Purkinje Eyetracker

Corneal and limbus eyetrackers can record very small eye movements, but their accuracy is poor. This inaccuracy arises from eye translation movements, which are indistinguishable from eye rotation movements. For example, 0.1 mm of eye translation causes approximately a 1° artifactual signal in the eye-rotation record from a corneal-reflection or limbus eyetracker.

The double-Purkinje method of eyetracking eliminates the translation artifact from the eye-rotation measurement. It is based on the use of a pair of reflections from optical surfaces of the eye. These reflections move by the same amount with eye translation but differentially with eye rotation. By monitoring the spatial separation of these two images, eye rotation can be measured accurately without being confused by translation. Similarly, eye translation can be measured accurately without being confused by eye rotation.

A. Purkinje Images

The virtual image formed by light reflected from the anterior surface of the cornea is known as the first Purkinje image, or corneal reflex [see Fig. 1(a)]. A second Purkinje image, formed by the component of light reflected from the posterior surface of the cornea, is almost coincident with the first Purkinje image. The light that is not reflected from either of these surfaces passes through the cornea, through the aqueous humor, and then through the lens of the eye. The third Purkinje image, a virtual image formed by the component of the light reflected from the anterior surface of the

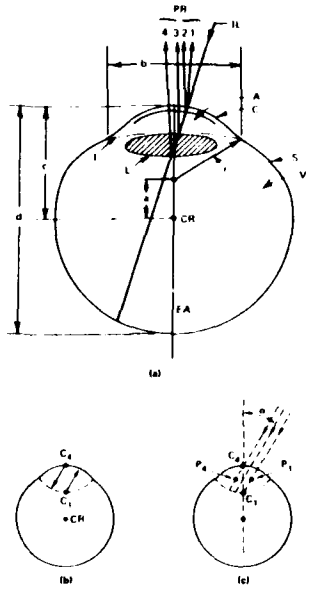

Fig. 1. (a) Schematic of the eye: *IL*, incoming light; *PR*, Purkinje reflections; *A*, aqueous; *C*, cornea; *S*, sclera; *V*, vitreous; *I*, iris; *L*, lens; *Cr*, center of rotation; *EA*, eye axis ($a \simeq 6$ mm, $b \simeq 12.5$ mm, $c \simeq 13.5$ mm, $d \simeq 24$ mm, $r \simeq 7.8$ mm). The transmitted component of *IL* is refracted at each surface of the eye, as is each reflected component as it passes back through these surfaces. For simplicity, however, this refraction is ignored in the figure. (b) The first and fourth Purkinje mirrors essentially form a clamshell arrangement. C_1 and C_4 are the centers of curvature of the two respective mirrors. (c) Location of the first and fourth Purkinje images, P_1 and P_4, for collimated input light at an angle α from the optic axis of the eye.

lens, is much larger and more diffuse than the other Purkinje images and is formed in a plane far removed from the plane of the other images. The fourth Purkinje image is formed by light reflected from the posterior surface of the lens at its interface with the vitreous humor. The rear surface of the lens acts as a concave mirror, forming a real image of the source.

The equivalent mirror surfaces that cause the first and fourth Purkinje reflection components form a basic clamshell arrangement. That is, the center of curvature for the first Purkinje mirror C_1 and the center of curvature for the equivalent fourth Purkinje mirror C_4 lie approximately within the opposite mirror surfaces [Fig. 1(b)]. Collimated light impinging on the eye at an angle α forms Purkinje images as shown in Fig. 1(c). The first Purkinje image, labeled P_1, lies along the incoming ray passing through C_1 and at a distance equal to the focal length of the cornea (i.e., one-half of its radius of curvature). The fourth Purkinje image, labeled P_4, lies along the ray passing through C_4 and at a distance equal to the focal length of the equivalent fourth Purkinje mirror (one-half of its radius of curvature). Because of the basic clamshell arrangement, both images lie almost exactly in the same plane, namely the pupil plane of the eye.

Although the fourth Purkinje image is almost the same size and is formed in almost the same plane as is the first Purkinje image, it is very dim because the difference in the refractive index between the lens and the vitreous humor is very small; the intensity of the fourth Purkinje image is less than ½% that of the first Purkinje image.

A more detailed discussion of Purkinje image formation and movement is given in Ref. 2.

B. First-Generation Eyetracker

An early double-Purkinje-image eyetracker system is shown in Fig. 2. A light source S is imaged by lens L_1 onto stop S_1, which defines the effective size of the light source. Stop S_1 is in the focal plane of lens L_2. Therefore, an image of S_1 is formed in the focal plane of lens L_3, which is made coincident with the pupil plane of the eye.

First and fourth Purkinje images are formed of stop S_2, which is located in the focal plane of lens L_3. Stop S_2, therefore, appears to the eye at optical infinity. All the light emerging from stop S_2 passes through the image of S_1 formed at the eye.

First and fourth Purkinje images of stop S_2 are formed approximately in the plane of the eye pupil. Light from these images is, in turn, reflected by dichroic mirror *DC*, reimaged by lens L_4, reflected by mirror *M*, and divided by beam splitter *BS*, to form two pairs of images. A_4 is a diaphragm containing a small round hole positioned to pass the fourth image to quadrant photocell P_4. This diaphragm, which is attached to P_4, blocks the light from the first Purkinje image. Beam splitter *BS* reflects about 10% of the incident light

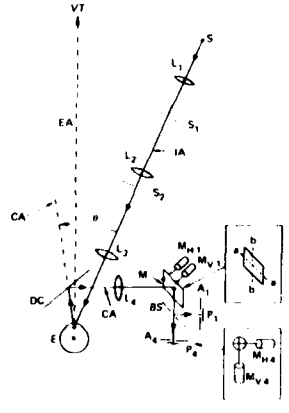

Fig. 2. Schematic of the first-generation eyetracker optical system: *E*, eye; *VT*, visual target; *IA*, input axis; *CA*, collecting axis; *CA'*, extension of collecting axis; *S*, light source; S_1, stop imaged at pupil of eye; S_2, source of Purkinje pattern, imaged at infinity; *DC*, dichroic mirror; *M*, front surface mirror; $M_{H,1}$ and $M_{V,1}$, motors that drive *M* in horizontal (yaw) and vertical (pitch) directions, respectively; $M_{H,4}$ and $M_{V,4}$, motors that drive P_4 in horizontal and vertical directions, respectively; *BS*, beam splitter; P_1 and P_4, quadrant photocells; A_1 and A_4, apertures in front of P_1 and P_4, respectively.

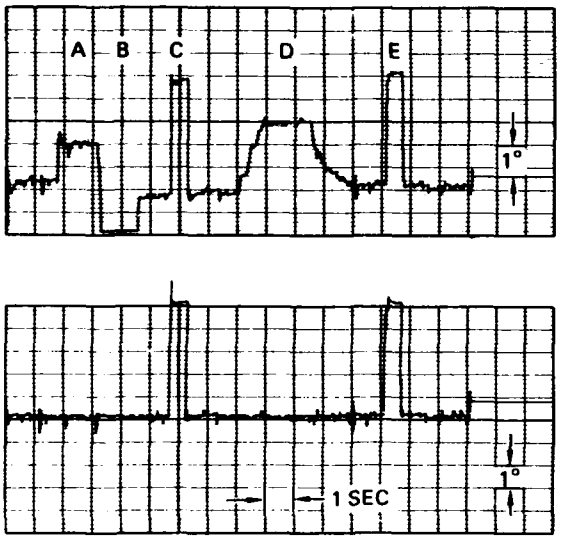

Fig. 3. Upper: horizontal eye movements recorded from first Purkinje image tracker while the subject fixates a target at infinity. Lower: simultaneous record from the fourth Purkinje image output. The upper track shows the wandering baseline, typical of corneal image trackers. During periods *A* and *B*, the subject leaned first one way and then the other way in the biteboard. During period *D*, the biteboard was translated laterally by ≃0.3 mm and then returned to its original position. Note the stability of the lower record during each of these intervals. During intervals *C* and *E*, the subject made voluntary eye movements of 5°.

toward another quadrant photocell P_1, which detects the first Purkinje image. Diaphragm A_1 is positioned to block all light except that from the first Purkinje image.

Mirror M is pivoted at its center and is driven in yaw (around axis *bb*; see inset) and pitch (around axis *aa*) by motors $M_{H,1}$ and $M_{V,1}$, respectively, which move to maintain the first Purkinje image centered on photocell P_1. Control signals that drive these two motors are derived from signals from the four sectors of P_1, which are arranged so that P_1 functions simultaneously as a horizontally oriented split-field cell and as a vertically oriented split-field cell.

Photocell P_4 is translated horizontally and vertically by motors $M_{H,4}$ and $M_{V,4}$, which move to keep the fourth Purkinje image centered on P_4 (see inset). Control signals that drive $M_{H,4}$ and $M_{V,4}$ are derived from the four quadrants of P_1, which also operates simultaneously as a horizontally and vertically oriented split-field cell.

Mirror M thus maintains the first Purkinje image stationary on photocell P_1, which is spatially fixed, while photocell P_4 is servocontrolled to track movement of the fourth Purkinje image relative to the first Purkinje image.[3]

If the eye translates, mirror M is automatically repositioned to maintain the first Purkinje image centered on P_1; the same movement properly repositions the fourth Purkinje image as well, and no movement of P_4 results. If the eye rotates, however, the images move differentially, and the position of P_4 changes accordingly. The position of P_4 thus indicates the separation between the first and fourth Purkinje images and is a measure of the two-dimensional (2-D) angular position of the eye.

The signals that drive the servos are generally referred to as error signals; the servos move until the error signals become zero. The error signals could themselves provide a direct measure of image movement without the servos, but in that form of system (generally referred to as open loop) the magnitudes and the linearity of the output signals are very sensitive to factors such as component drift and change in gain in both the photodetectors and amplifiers, variation in light sensitivity across the face of the photodetectors, and the uniformity, shape, and brightness of the light pattern. The servos, by maintaining each image fixed at an electrical null position on its respective photocell, eliminate the sensitivity to these parameters and result in a much more stable system.

Figure 2 is actually a schematic of the first-generation eyetracker described in Ref. 2.

C. Demonstration of Translation Insensitivity

Figure 3 shows the horizontal motion of the eye while fixating a target. The top record is the horizontal motion of the 2-D mirror driven from the first-Purkinje-image cell. The bottom record is the horizontal movement of the fourth-Purkinje-image photocell [or the movement of the mirror driven by the stationary fourth Purkinje photocell in the new system (see Fig. 4)]. The first Purkinje record has a wandering baseline, typical of corneal (or limbus) eyetrackers, that results from translation-induced errors, whereas the signal from the fourth cell is independent of translation effects.

For the record of Fig. 3, a tight fitting dental plate (biteboard) was used. During period A, the subject was asked to lean to the left in the biteboard, and during period B to lean to the right. Note that whereas the lower record is immune to such movement, the upper record shows an output variation of almost ±2°, indicating a movement of the head with respect to the biteboard of approximately ±0.2 mm. During period D, the subject's head was translated approximately 0.3 mm to the left (with respect to the instrument) and then returned to its original position. Note the 3° output variation in the upper record and again the stability of the lower record (taken from the fourth Purkinje image output). During periods C and E, the subject made voluntary eye movements of 5° amplitude indicating the ability of both systems to record actual rotation movements of the eye.

Figure 3 indicates the difference between sensitivity and accuracy. A corneal, or limbus, tracker can detect very small eye movements, but its accuracy, or repeatability, is limited by the artifactual effects produced by translation movements of the eye. We have recorded drifts of 1–2° that are indistinguishable from rotation

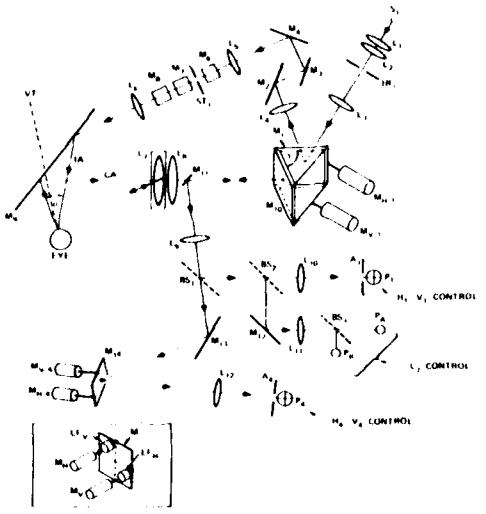

Fig. 4. Schematic of new eyetracker system: S_1, IRLED source; IR_1, adjustable iris conjugate with eye pupil; M_1 and M_{10}, coupled front-surface mirrors under control of motors $M_{H,1}$ and $M_{V,1}$; γ, angle between mirrors M_1 and M_{10}; M_2, M_3, M_4, M_6, M_7, M_8, M_{11}, M_{12}, and M_{13}, front surface mirrors (mirrors M_2, M_3, M_4, and M_5, not shown, are used in different combinations to alter the angle θ of the incoming illumination); M_{14}, front-surface mirror driven by motors $M_{V,4}$ and $M_{H,4}$; M_9, dichroic mirror; BS_1, 90/10 pellicle beam splitter; BS_2 and BS_3, 50/50 beam splitters; P_1 and P_4, quadrant photocells; A_1 and A_4, apertures in front of P_1 and P_4, respectively; P_A and P_B, photocells in automatic focus-detection circuit; VT, visual target; IA, input axis; CA, collecting axis; stop ST_1, source of Purkinje image pattern; LF_H and LF_V, linear followers.

of 1–2° during a recording span of less than 1 min even with the head held rigidly by a tight-fitting dental-impression plate with the extra support of a forehead rest. In this case, translation-induced effects must be attributable in large part to movements of the eye within its socket.

III. Second-Generation Eyetracker

The new double-Purkinje-image eyetracking system is shown in Fig. 4. This version, which combines many substantial improvements over the first-generation instrument, greatly extends its performance and is easier to use.

A. Input Optics

S_1 is a solid-state light source with a narrow spectral band centered at 0.93-μm wavelength. Light from S_1 is electronically chopped at high frequency (4 kHz) to avoid the effects of room light and to use ac-coupled amplifiers in the Purkinje image servosystems thereby improving stability and decreasing noise.

Lenses L_1 and L_2 image S_1 into the plane of an iris diaphragm IR_1, which is conjugate with the pupil of the subject's eye. Lens L_3 is positioned one focal length from the iris so the light emerging from L_3 is collimated. This light is reflected from servoed mirror M_1 and imaged by lens L_4. Assume for the moment, however, that mirror M_1 is fixed.

Lens L_5 is positioned one focal length from the image of the light source formed by lens L_4. The required pathlength ($f_4 + f_5$) between lenses L_4 and L_5 is obtained by the multiple reflections provided by mirrors M_2, M_3, and M_4. An odd number of reflections from these mirrors provides an inversion of the horizontal component of the input light path. This inversion is necessary for the proper functioning of mirror M_1, by means of which, as described later, the input light is made to track automatically any change in eye position.

Mirrors M_6, M_7, and M_8 form a Dove mirror system to provide an inversion of the vertical component of the illumination system, which is also necessary for proper input-light tracking. Within the Dove mirror system is a stop ST_1, a circular aperture approximately 2.54 cm (1 in.) in diameter. This aperture determines the size and shape of the Purkinje images formed at the eye and is in the focal plane of lens L_6. Thus, light emerging from lens L_6 is collimated with respect to the image of the aperture. The eye is in the focal plane of lens L_6 and is illuminated by the light coming from the light emitting diode. Dichroic mirror M_9 reflects both the illumination light and the light reflected from the first and fourth Purkinje images that form in the subject's eye.

B. Output Optics

The Purkinje images are formed in the pupil plane of the eye, which is in the focal plane of output lens L_7. Thus, light from the Purkinje images is collimated between lenses L_7 and L_8. The light that passes through lens L_8 is reflected from mirror M_{10} onto mirror M_{11}, which is in the focal plane of lens L_8.[4] Because lenses L_7 and L_8 have the same focal length, a unity magnification image of the pupil plane of the eye is formed at mirror M_{11}.

Mirror M_{11} is in the focal plane of lens L_9. Therefore, the light emerging from lens L_9 is collimated. Beam splitter BS_1 reflects approximately 10% of the incident light toward beam splitter BS_2. The remaining light passes through BS_1 to front-surface mirror M_{13}. Beam splitter BS_2 reflects and transmits approximately equal amounts of light. The transmitted light is imaged by lens L_{10} onto the four-quadrant detector P_1, which is in the focal plane of L_{10}. P_1 is therefore in a plane conjugate to mirror M_{11} and the pupil plane of the eye; aperture A_1 defines the size of field seen by P_1. Thus, when the first Purkinje image is at one particular point on mirror M_{11} (or in the pupil plane of the eye), it will fall on the center of the four-quadrant photodetector. If the image tends to move away from this point, the image at the detector will move, and the resulting error signals will drive servomotors $M_{H,1}$ and $M_{V,1}$ to reposition mirror M_{10} (and mirror M_1). The mirror is repositioned in yaw and pitch to bring the first Purkinje image to its initial point on mirror M_{11} and thus on the

photodetector. In this way, the image of the eye formed at mirror M_{11} always has its corneal reflection in the same location.

The light reflected from beam splitter BS_2 reflects from front-surface mirror M_{12} and is imaged by lens L_{11} (and split by a 50/50 beam splitter BS_3) onto two focus-detecting photodiodes P_A and P_B. These photodiodes are displaced axially approximately 0.5 cm on either side of the plane of focus of the first Purkinje image and, being small in size, measure light-flux density along the axis of the imaging system. When the eye is in the correct position axially, each of these photodiodes receives the same amount of light. If the eye moves axially, one or the other of these photodiodes receives more light, and the difference in light level generates an error signal for a servomoter that drives the carriage containing lens L_7. As described later, lens L_7 is repositioned so the two photodetectors continually receive equal amounts of light. This ensures that the first Purkinje image is always in focus on P_1 in spite of axial eye movement.

The light transmitted by beam splitter BS_1 reflects from mirror M_{13} onto the servoed mirror M_{14} and is collected by lens L_{12}. At the focal plane of lens L_{12} is a second four-quadrant photodetector P_4, which receives the fourth Purkinje image; aperture A_4 defines the size of field seen by P_4. Signals derived from quadrant cell P_4 control motors $M_{H,4}$ and $M_{V,4}$. These motors move mirror M_{14} in yaw and pitch to keep the fourth Purkinje image centered on P_4.[5]

Opposite each mirror motor is mounted a linear motion follower LF with a sensitivity better than 1 μm (see inset of Fig. 4). These motion sensors are used in a local internal servo feedback loop in each driver circuit to achieve high frequency response and to minimize hysteresis and dead zone. Signals from $LF_{H,1}$ are used in the servo loop that drives motor $M_{H,1}$, and signals from $LF_{V,1}$ are used in the servo loop that drives motor $M_{V,1}$. Similar motion sensors are used in conjunction with drive motors $M_{H,4}$ and $M_{V,4}$.

The direction of the eye axis, i.e., the angle of gaze, is derived directly from $LF_{H,4}$ and $LF_{V,4}$ signals, as described earlier. Signals from $LF_{H,1}$ and $LF_{V,1}$ represent the horizontal and vertical positions of the first Purkinje image, which moves in response both to eye translation and eye rotation. By properly combining the signals from $LF_{H,4}$ and $LF_{V,4}$ with those from $LF_{H,1}$ and $LF_{V,1}$, one can also accurately track the translational position of the eye.

C. Automatic Input-Path Tracking

The new instrument is designed to permit up to a centimeter of eye position variation in all dimensions: horizontal; vertical; and axial. For a large axial variation to be tolerated, it is necessary to incorporate automatic focus into the eyetracker (see the next section on automatic focus). For large lateral variations to be tolerated, either a large input beam must be used, so the eye never moves out of the beam, or the input light path must track eye position automatically, in which case a small light source can be used. The latter option was chosen because it offers many advantages: less total light energy directed toward the eye; a crisper fourth Purkinje image because of less stray light; and improved automatic capture because the first Purkinje tracker can sometimes lock onto the iris if it is illuminated.

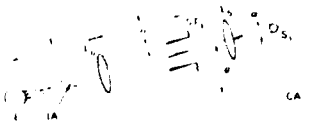

Fig. 5. Translation of the source S_1, or source image S_1', moves the image at the eye but does not change the angular separation θ between the input axis IA and collecting axis CA. A cone of size α will emerge from each point of the pattern in stop ST_1, where α is the angular size of the source image S_1' as seen from lens L_5.

For automatic input-path tracking, mirror M_1 (in the input path of Fig. 4), which was assumed fixed in the earlier discussion, is used to keep the illumination beam centered on the pupil. For this purpose, mirror M_1 is rigidly connected to, and therefore moves in synchronism with, mirror M_{10}.

To understand how the input light is made to track eye position, note that, if the eye moves upward, the corneal reflection tends to move upward on detector P_1. Error signals generated by this photodetector reposition mirror M_{10} to maintain the corneal image centered on M_{11}. Motion imparted to M_{10}, however, also repositions mirror M_1; this automatically deflects the illumination beam upward to track the corneal reflection. However, the illumination tracking cannot be perfect with respect to the pupil of the eye because P_1 tracks the corneal reflection, which moves with respect to the eye pupil when the eye makes rotational movements. Nevertheless, the design is such that the tracking error is less than 1 mm with eye translation of $\pm$0.5 cm in any direction and with eye rotations of 15° in all directions (30° diam field), that is, the input illumination beam tracks the center of the pupil to within 1 mm over this range.

A critical requirement of the input-light tracking system is that a shift in the input light path must not cause any change in the angle of the input axis IA with respect to the eye axis. Any such change would alter the separation of the Purkinje images and therefore be interpreted as an eye rotation. This situation is avoided as follows.

Figure 5 shows the light entering the eye directly at an angle θ to the collecting axis. (For simplicity, the dichroic mirror is not shown.) The input system consists essentially of lens L_6 located at its focal length from the eye and stop ST_1 located one focal length away from L_6. Stop ST_1 therefore appears to the eye to be at infinity. Stop ST_1 is illuminated by S_1', which is an image of iris IR_1 and is in the focal plane of lens L_5. The light cones emerging from each point of ST_1 are collimated by lens L_6, and their intersection at the eye is an image of S_1' and therefore of iris IR_1.

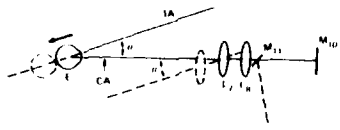

Fig. 6. Focus adjustment by translating lens L_7 along a path parallel to the input axis IA. This method of focus adjustment maintains constant optical magnification over the focus range and maintains a constant final image position when the eye translates along the input axis. CA, collecting axis; θ, angle between CA and IA.

If iris IR_1 were translated in its own plane, its image S_1', and hence the image of S_1' at the eye, would similarly translate, but the collimated ray bundles from each point of ST_1 would not change their angular orientation, as desired. It is therefore possible to achieve the desired input tracking simply by translating the iris. However, that would require yet another 2-D servosystem. Instead, the same effect is achieved by placing mirror M_1 in the collimated light path between lenses L_3 and L_4 (in Fig. 4) and attaching it rigidly to mirror M_{10}, as described above. The required movement sensitivity in the input light path is obtained by the proper choice of angle γ (see Fig. 4) between mirrors M_1 and M_{10}.

D. Automatic Focus

To obtain the desired 1 cm of allowed axial variation in eye position, an automatic focus system tracks the axial position of the eye. Without automatic focus, intolerable blurring of the Purkinje images would occur at the quadrant photocells.

The automatic focus system must meet two stringent requirements: First, any change in focus must not cause any change in optical magnification. A change in magnification would result in a change in separation of the two Purkinje images and, therefore, be interpreted as an eye rotation. Figure 6 shows the eye and the two output lenses L_7 and L_8; again, for simplicity, the dichroic mirror is not shown. The Purkinje images are in the focal plane of lens L_7. Because the light between lenses L_7 and L_8 is collimated, the eye and lens L_7 can both move along axis CA without any change in magnification in the final image, as long as the distance between the eye and lens L_7 remains constant. The first step in automatic focus, therefore, is to have the axial position of lens L_7 track the axial position of the eye.

The second requirement is that the input light not shift if the eye translates along the input-light axis IA. In that case, the input light is already aimed directly at the eye, and any shift would move the light away from the eye. In other words, the automatic focus system must be designed so eye translation along the input axis does not cause any shift in mirror M_{10}, which in turn requires that there be no change in the position of the first Purkinje image. This is achieved by shifting lens L_7 not along axis CA, but along the path parallel to the input-light path IA, as shown by the dashed line of Fig. 6. Again, because the light between lenses L_7 and L_8 is collimated, an equal lateral component of shift of the eye and lens L_7 will not change the position of the final image formed by lens L_8. A shift in eye position along any other axis will, however, shift the input-light path appropriately as well as activate the automatic focus system.

In Fig. 4 we noted that the signal that drives the focus servosystem derives from the difference in signals from photocells P_A and P_B. This signal is zero when the first Purkinje image is in focus on quadrant photocell P_1.

Output from the servosystem that drives L_7 provides a direct measure of the axial position of the eye. Combined with the horizontal and vertical eye position signals described earlier, the 3-D position of the globe can thus also be accurately tracked separately from the angular orientation of the globe.

E. Automatic Search

An automatic search of the field is made whenever the first Purkinje system becomes unlocked, as indicated by an improper light level falling on photocell P_1. In this case, the first Purkinje mirror is made to sweep in an increasing spiral from the central position, and the focus servosystem returns to its central position. On the average, recapture occurs about ½ sec after the initiation of a search action. When successful capture has been achieved by the first Purkinje system, the focus servosystem is reactivated, and a small-field spiral search is initiated by the fourth Purkinje system. (With the first Purkinje system locked, the fourth Purkinje image falls within a small, well-defined area.) Again, the average capture occurs about ½ sec after initiation of a search action, for a total average search-and-capture of about 1 sec. Separate light-level detectors in the fourth Purkinje system indicate when the fourth system is operating normally. A search for the fourth image is automatically initiated whenever the fourth light level is out of range.

A separate output signal indicates whenever the first or fourth Purkinje tracker is unlocked for any reason. The signal can be used to ignore those portions of the eye records in manual or automatic processing of the data.

IV. Optometer Principles

A. General

Reference 1 describes the basic form of the optometer that is combined with the double-Purkinje-image eyetracker in the 3-D instrument. In this section, we discuss the basic principles of the optometer.

Figure 7 is an optical diagram of the eye viewing a point source through a small aperture. In Fig. 7(a), the refractive power of the cornea and lens are such that the point is sharply imaged on the retina. In this case, if an aperture were moved from position A to position B, different bundles of rays from the source would strike the retina, but the illuminated retinal spot would be stationary. In Fig. 7(b), the refractive power of the eye is too small, and the retinal spot moves from position A' to B' in response to aperture movement from A to B.

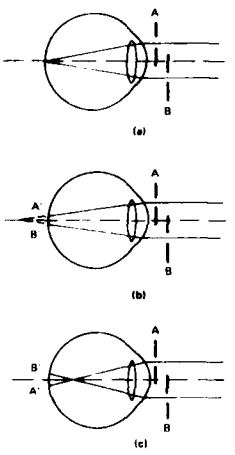

Fig. 7. Imaging a point target at infinity through a small aperture that alternates between two positions, A and B. The intercepted-ray position at the retina will be stationary or will move with or move opposite to the aperture, respectively, according to whether the eye is focused for infinity (a), beyond infinity (b), or closer than infinity (c).

Conversely, in Fig. 7(c), the refractive power of the eye is too great, and the retinal spot moves from A' to B' (i.e., in the opposite direction) in response to aperture movement from A to B. The object plane conjugate to the retina can be found by changing the distance of the source, according to the polarity of the image movement, until the retinal image is stationary. The optometer performs this function automatically and continuously.

Figure 8 illustrates the basic optometer configuration. Instead of a mechanical aperture positioned close to the eye, an optical projection system achieves the same effect. Two adjacent, near-ir light sources, S_2 and S_3, which have a narrow spectral band centered at 0.93-μm wavelength, are located in the focal plane of lens L_1.[6] An image of the light sources is formed in the plane of the pupil of the eye, which is at the focal plane of lens L_2. The light sources flicker on and off alternately at a rate of 400 Hz. Thus, light enters the eye first through one small area of pupil (the image of the first light source) and then through an adjacent area of the pupil (the image of the second source). This is equivalent to two alternating aperture positions.

Stop ST_2, which is illuminated alternately by sources S_2 and S_3, appears to the eye at a virtual distance

$$L = (f_2)/|1 - [d/(f_2)]|, \tag{1}$$

where L, d, and f_2 (the focal length of lens L_2) are in meters. To focus stop ST_2 on the retina requires an accommodation level

$$D_E = \frac{1}{L} = \frac{1}{f_2}\left(1 - \frac{d}{f_2}\right), \tag{2}$$

where D_E is in diopters. We use the convention that the refractive power of the eye is stated relative to its power when accommodated for infinity (i.e., when $d = f_2$, $D_E = 0$ diopters). As the eye changes its refractive power, stop ST_2 is maintained in focus on the retina by adjusting d, whose position is a direct measure of the instantaneous refractive power of the eye. Note from Eq. (2) that D_E, measured in diopters, is linearly related to the distance d measured in meters.

Stop ST_2 is moved along the optical axis in response to the movement of the image of stop ST_2 on the retina. This movement is detected by reimaging the retinal image onto a split-field photocell SFP and sensing lateral movement of the image in synchronism with the alternation of light sources S_2 and S_3. If stop ST_2 is in focus on the retina, the image will be stationary. If the image is out of focus, it will appear to move either in phase or out of phase with the alternation of the light source, as illustrated in Fig. 7.

The image formed at the photocell derives from light reflected from the retina, which passes back out through the pupil of the eye. This light is reflected by dichroic mirror M and then by beam splitter BS. If ST_2 is in focus on the retina, lens L_3, which is identical to lens L_2, forms an image of the retinal image in a plane that is conjugate with stop ST_2 (i.e., at plane RI, which is at a distance d from lens L_3). For clarity, lens L_3 is drawn adjacent to lens L_2, as though the dashed portion W of the output path were of zero length; actually, L_3 is located at the same optical distance from the eye as is L_2. Split field photocell SFP could be located in plane RI except that it is necessary first to block the corneal reflection, which is much brighter than the reflected retinal image. Thus, the image in plane RI is relayed by a pair of fixed lenses L_4 and L_5. With L_4 and L_5 separated by a distance equal to twice their focal length, the retinal image formed in plane RI is relayed a distance equal to four focal lengths (see next section), as shown in Fig. 8, in which plane SFP is located. An image of the plane of the pupil is obtained in the focal plane of lens L_4, which is conjugate also to the plane of the light sources S_2 and S_3. A small corneal stop (CS) placed in this plane blocks the very small but bright corneal reflection of sources S_2 and S_3.

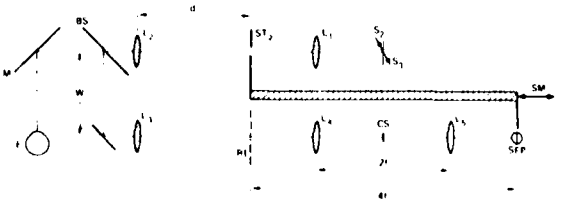

Fig. 8. Basic optometer arrangement: S_2 and S_3, IRLEDs; ST_2, stop that is imaged on the retina; M, dichroic mirror; BS, beam splitter; CS, corneal stop; SFP, split-field photocell. ST_2 and SFP are linked mechanically to slide SM. The number of diopters of accommodation required by the eye to focus on ST_2 is linearly related to the distance d between ST_2 and L_2. When ST_2 is in focus on the retina, the retinal image is also reimaged at plane RI, which is relayed by fixed lenses L_4 and L_5 to the plane of SFP. For simplicity, L_3 is drawn opposite L_2, although the entire output path should be shifted to the left by the distance W.

Stop ST_2 and the SFP are mechanically linked. Thus, when stop ST_2 is in focus on the retina, the retinal image will be conjugate with, and therefore stationary on, the split-field cell. If ST_2 is out of focus, movement of the image on the retina in one phase or the other will drive the slide SM in the appropriate direction until the error signal is zero, and the image is stationary on the retina and therefore on the photocell. If the servosystem has a faster response than the accommodation system of the eye, the instantaneous position of the slide (i.e., distance d) will provide an accurate measure of the instantaneous refractive power of the eye.

B. Optometer Range

From Eq. (2), we see that $D_E = 1/f_2$, when $d = 0$. Thus, the maximum measurable diopters is equal to the focal length (in diopters) of lens L_2. To measure an accommodation level up to +20 diopters, for instance, lens L_2 would require a focal length of 1/20th m, or 50 mm. The problem with such a short focal length lens is that it must be brought very close to the eye, and there is very little room for other optical elements that might be needed.

A way to increase this distance and the diopter range at the same time is to use an image of stop ST_2 instead of the stop itself. The problem with a real stop, of course, is that it cannot pass through the lens. That is, we cannot achieve negative values of the distance parameter d. But an image can pass through the lens, and in that way the power of the instrument can be increased beyond the power of lens L_2. [Equation (2) holds exactly even for negative values of d.] This fact is important in combining the eyetracker and optometer, which is discussed in the next section.

V. Combined Three-Dimensional Instrument

The major task in building a composite instrument was to combine an optometer instrument of the form shown in Fig. 8 with the eyetracker shown in Fig. 4. To help the reader appreciate how the merging was achieved, we must discuss briefly a certain basic feature of a telescope.

The simplest telescope consists of a pair of positive lenses separated by a distance equal to the sum of their focal lengths. Although telescopic systems have undergone extensive study and many practical developments, here we are concerned only with certain properties and uses of the telescope as a relay system.

With a pair of lenses separated by the sum of their focal lengths, it is easy to show that the object and image distances, p and q, measured from each lens, as shown in Fig. 9, have the following linear relationship:

$$q = f_2\left(1 + \frac{f_2}{f_1}\right) - \left(\frac{f_2}{f_1}\right)^2 p, \tag{3}$$

where f_1 and f_2 are the focal lengths of the two lenses. As a result, both the axial magnification ($\Delta q/\Delta p$) and the lateral magnification ($M = f_2/f_1$) are constant, independent of distance p. Although apparently not well known, it is therefore possible with this configuration (for the case $f_2 = f_1$) to achieve imaging with neither

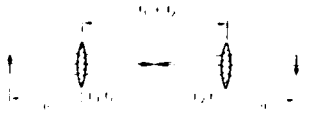

Fig. 9. Telescope configuration. With two lenses separated by the sum of their focal lengths, the object and image distances, p and q, are linearly related, and lateral magnification is independent of p.

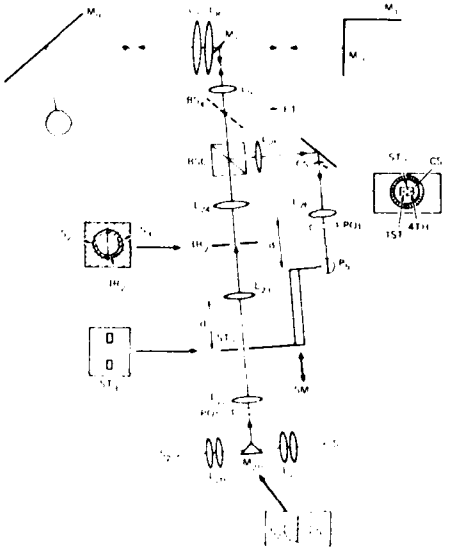

Fig. 10. Merging the two instruments. The instruments are merged by means of beam splitter BS_4. ET, remainder of the eyetracker system; BSC, polarizing beam splitter cube; S_2 and S_3, IRLEDs; M_{20}, 90° mirror that merges the images of S_2 and S_3; ST_3, stop that is imaged on the retina; IR_2, adjustable iris conjugate with the eye pupil plane; P_5, split-field photocell on which the retinal image falls; CS, corneal stop; POL_2 and POL_3, polarizers that reinforce the input and output polarization directions of BSC; ST_3 and P_5 are linked mechanically to slide SM.

axial nor lateral distortion (at least to a first-order approximation); compare this case with single-lens imaging, in which axial and lateral magnification both vary with the object-to-lens distance (see Fig. 3 of the accompanying paper[7]).

Of specific interest to this discussion is that the object and image distances are linearly related, even for $f_2 \neq f_1$. In fact, just as Eq. (2) is true for an object on the far side of the lens (negative values of d), so too it is readily shown that Eq. (3) is true for an object (or an image of an object) that falls between the two lenses of Fig. 9 and even beyond the right-hand lens (i.e., negative values of p). Thus, a telescopic relay in the optometer path does not alter the linear relation between eye diopters and the movement of stop ST_2.

In Fig. 4, lenses L_7 and L_8 together form a unity magnification image of the Purkinje reflections at mirror M_{11}, which is the focal plane of lens L_9. Looked at another way, lens L_7 is a focal distance from the pupil

plane of the eye and plays the role of lens L_2 in Fig. 8, while lenses L_8 and L_9, which are separated by the sum of their focal lengths, together form a (nonunity ratio) telescope system. By merging the optometer with the eyetracker on the distal side of lens L_9 as viewed from the eye, we benefit from the first-Purkinje-image stabilization provided by mirror M_{10}, while maintaining the linear relation of Eq. (2) between eye diopters and servo motion. We can also obtain a large diopter range even though lens L_7 is of relatively long focal length; see Sec. IV.B. The main disadvantage of this scheme is that lenses L_7, L_8, and L_9 are now common to the input and output paths of the optometer. Any reflection of optometer input light from these lens surfaces that enters the optometer output path can cause serious artifact signals because the total light reflected from the fundus of the eye is extremely small. Elimination of these reflections requires special care.

A schematic of the composite instrument is shown in Fig. 10. The two instruments are merged via beam splitter BS_4, which is mounted between lens L_9 and beam splitter BS_1 (see Fig. 4). Although BS_4 reflects the optometer light at right angles to the plane of the paper of Fig. 4, BS_4 is shown as transmitting, rather than reflecting, so the optometer and relevant eyetracker optics can be drawn in a single plane.

A. Optometer Input Path

Light sources S_2 and S_3 are imaged by lens pairs L_{20} and L_{21} onto a right-angle mirror M_{20}, which causes two half-disks of light to appear side by side, as shown in the lower inset to Fig. 10. The two half-disks of light are energized out of phase. An image of this flickering light pattern, which is in the focal plane of lens L_{22}, is formed on iris diaphragm IR_2 located in the focal plane of lens L_{23} and also in the focal plane of lens L_{24}. (Lenses L_{23} and L_{24}, which are identical and are separated by twice their focal length, form a unity ratio relay lens.) Another image of the light sources S_2 and S_3 is thus formed on mirror M_{11}, which, as explained earlier, is conjugate to the pupil plane of the eye. The diameter of the light source pattern at the eye pupil plane is adjustable by means of iris IR_2 (see inset, Fig. 10).

Stop ST_3 and lens L_7 together are functionally equivalent to stop ST_2 and lens L_2 in Fig. 8, except that they are separated by two relay lens pairs, (L_8, L_9) and (L_{23}, L_{24}), in series. (Relay lens pairs in series have the same linearity properties as a single lens pair.) With stop ST_3 positioned so that its image is in the focal plane of L_9, light from ST_3 reaching lens pair L_7 and L_8 is collimated, and another image of ST_3 is formed halfway between L_7 and the eye, a distance $f_7/2$ from the eye (which represents nine diopters of refractive power). As ST_3 moves farther from (or closer to) L_{23}, the final image moves farther from (or closer to) the eye, i.e., to a position of less (or more) dioptric power.

Stop ST_3 is a narrow slit with its center blocked (see the inset on the left of Fig. 10). The reason for blocking the center is that very bright, on-axis, input light would be reflected directly back by mirror M_{11} (after reflection from M_{11} to M_{10} and then back toward L_8) and could cause a serious artifact in the optometer output signal.

B. Optometer Output Path

Lenses L_{25} and L_{26} are conjugate with lenses L_{24} and L_{23}, respectively. A corneal stop CS is located in a plane conjugate with iris IR_2. If stop ST_3 is in focus on the retina, an image of the retinal image is formed at a distance d from lens L_{26}. The split-field cell P_5 is placed in this plane, as shown in Fig. 10. If ST_3 is out of focus on the retina, its image on the retina moves in synchronism with S_2 and S_3. This side-by-side motion is detected by P_5, and the resulting signal drives the slide containing ST_3 until the retinal image is again stationary.

Potentially large artifact signals can be generated in the optometer output by specular reflections of optometer input light from lenses L_7, L_8, L_9, and the cornea, which are common to the input and output paths of the optometer. This potentially serious artifact is eliminated by polarizing the optometer input light with a polarizing beam splitter cube BSC. Any specularly reflected light from lenses L_7, L_8, L_9, and the cornea has the same polarization as the input light and, therefore, will not be reflected into the optometer output path, but will pass directly back through the BSC.

Polarizers POL_2 and POL_3, shown in the optometer input and output paths in Fig. 10, are not logically necessary, although they are important for proper functioning. Polarizer POL_2 blocks the input light that would normally be reflected by BSC, thus substantially reducing the magnitude of light that may be rereflected from the external surface of BSC and that could reenter the output path. Further, because BSC is not a perfect polarizer, a certain amount of light is also scattered at its diagonal interface. POL_3 significantly reduces the amount of scattered light that enters the output.

C. Optical Isolation between the Two Instruments

Eyetracker light is blocked from the optometer by enlarging the corneal stop CS in the optometer output path. The inset on the right of Fig. 10 shows the Purkinje reflection from the optometer, labeled ST_3, and from the eyetracker, labeled 1st and 4th. The BSC prevents most of the optometer light that is reflected from the cornea from reentering the output path of the optometer. However, this reflected light is so bright that it is still necessary to use a corneal stop CS that is large enough to block the corneal image of ST_3. By enlarging the stop, as shown in the inset in Fig. 10, light from the first and fourth images from the eyetracker is also blocked. The stabilizing action of the eyetracker keeps the corneal reflection blocked by the stop CS even under conditions of eye rotation and/or trans. tion.

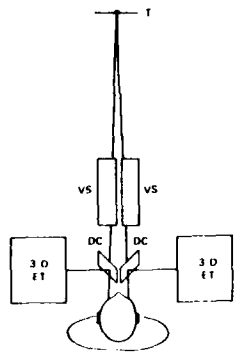

Fig. 11. Subject configuration for stimulating and recording 3-D eye movements: 3D-ET, 3-D eyetracker, which includes dichroic mirror *DC*; *VS*, 3-D visual stimulator; *T*, target.

D. Electrical Isolation of the Instruments

Most of the eyetracker light is eliminated from the optometer by the enlarged corneal stop as noted above. In the eyetracker, the effects of a bright corneal image of the optometer input falling on top of a weak fourth Purkinje image (in certain directions of gaze) are eliminated by a high-pass electrical filter, which creates a single-sideband system for the 4-kHz eyetracker signal. This filter eliminates any 400-Hz signals from the eyetracker channels. A combination of low-pass and bandpass filters removes from the optometer signal any residual 4-kHz eyetracker signals.

VI. Performance

A. Binocular Configuration

Figure 11 shows a binocular configuration with which the records of this section were taken. Each eye views a target *T* through a dichroic mirror (mirror M_9 in Fig. 4) and a 3-D visual stimulator *VS*. By means of three servocontrolled mirror and lens systems, *VS* can move the visual field horizontally and vertically independently and can vary the optical distance of the target without changing its brightness or size.[7] The *VS* also provides a location for an artificial pupil, if desired. Movements of each eye are monitored by a separate 3-D eyetracker. Two such stimulator and eyetracker instruments aligned side by side in a binocular configuration provide independent visual stimulation and recording from each eye. Figure 12 is a photograph of a pair of 3-D eyetrackers and visual stimulators arranged in such a binocular configuration.

The focus stimulator portion of *VS* can be used as a focus corrector for subjects who normally wear glasses. Although the eyetracker has been operated with subjects wearing glasses, it is not the preferred method of operation. The *VS* can adjust spherical power to suit the subject, and cylinder power can be corrected with standard ophthalmic cylinder lenses inserted near the artificial pupil plane.

B. Three-Dimensional Records

Single-eye recordings are adequate to illustrate the basic response of the instrument. In Fig. 13, the right eye was occluded, and the left eye *VS* caused a fixation target to be moved simultaneously in a sawtooth pattern vertically and in a sine-wave pattern horizontally both 8° peak to peak. At the same time, the focus stimulator

Fig. 12. The 3-D, binocular arrangement.

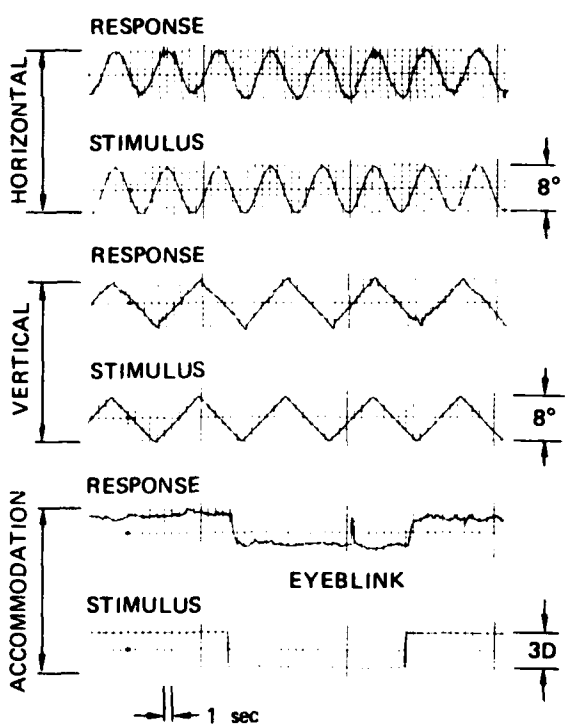

Fig. 13. 3-D, monocular recording made while the subject tracked a target moving horizontally according to an 8° sine wave, vertically according to an 8° sawtooth of different frequency, and in focus according to a 3-diopter square wave of still another frequency (right eye occluded).

altered the optical distance to the target between infinity (zero diopters) and a third of a meter (three diopters), according to a square-wave pattern. That is, the target movement in each dimension was independent of the form and frequency of the movement in the other dimensions.

C. Eyetracker and Optometer Response

The noise level in the X and Y channels of the 3-D eyetracker is less than 1 min of arc rms. The allowable range of eye movements varies from subject to subject, depending primarily on pupil size. A range of at least 20° is achieved easily with most subjects. The optometer has a range from −4 to +12 diopters and a noise level of approximately 0.1 diopter.

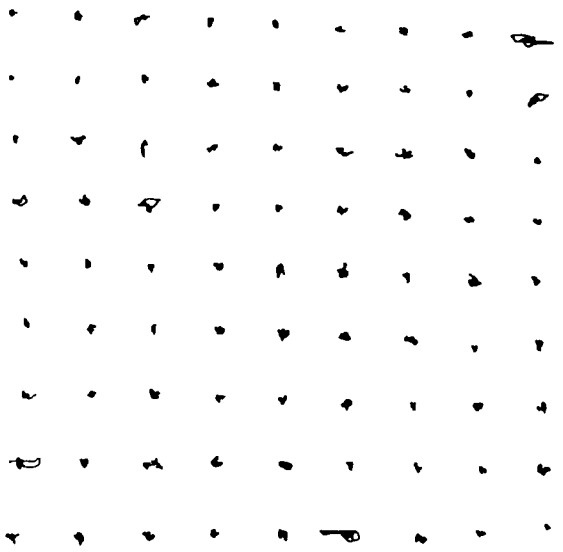

Fig. 14. Two-dimensional field plot; spacing between spots is 2°.

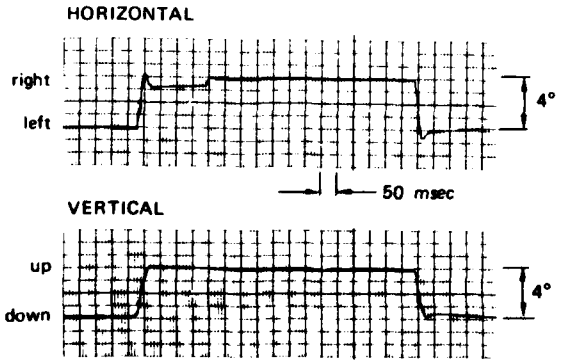

Fig. 15. Simultaneous horizontal and vertical eye movements, showing the general form of the response. Note the difference in horizontal and vertical eye movement velocities during the saccade.

Figure 14 is a 2-D field plot of the eyetracker made with an $X-Y$ recorder. The X and Y inputs were driven directly from the horizontal and vertical outputs, H_4 and V_4, of the fourth Purkinje tracker. For this plot, the subject moved his fixation voluntarily around a 9-by-9 matrix of bright points spaced 2° apart. The subject fixated on each point for several seconds; the pen was deenergized between fixation points.

Although there is a field distortion over large eye movements, repeatability is a few min of arc, that is, the plot retraces itself to that degree of accuracy even if the subject gets off the biteboard between plots.

The horizontal and vertical servoes have a frequency response approximately flat to 300 Hz and a maximum slewing rate greater than 1000°/sec. Figure 15 shows the eye response to a diagonal step change having 4° horizontal and vertical components. Note that the horizontal velocity in the first saccade is almost twice that of the vertical velocity—200°/sec vs 100°/sec. The servoes also have a lag of approximately 1 msec, which results in a 6-min of arc lag when tracking an eye movement of 100°/sec.

The dynamic response and the noise level of the eyetracker are adequate to achieve a stabilized-image disappearance of moderate contrast targets when the eyetracker signals are used to drive a CRT so that its pattern tracks the eye movements and thereby stabilizes the image on the retina.[8] Good disappearance capability has also been demonstrated using the 3-D stimulator to stabilize a fixed visual pattern in space.

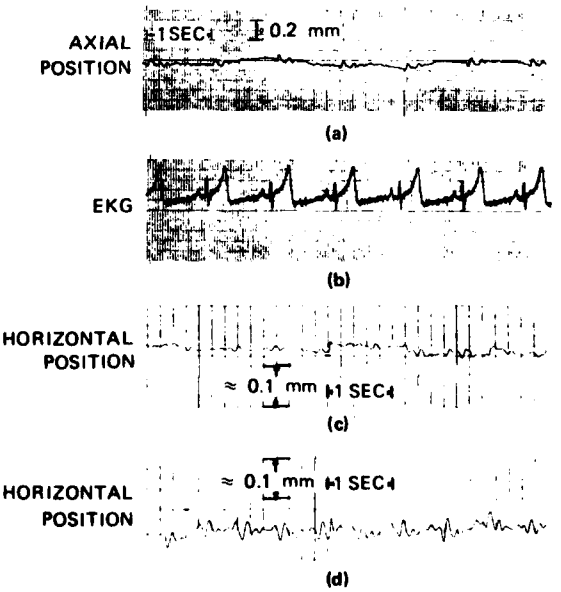

Fig. 16. Eye movement in response to heartbeat. These illustrate the sensitivity of the instrument in detecting 3-D translational as well as rotational motions of the globe. (a), (b) Axial eye motion and simultaneous EKG; horizontal eye motion (c) before and (d) after exercise.

D. Translation Sensitivity

The primary achievement of the Purkinje eyetracker is separation of the translation and rotation components of eye motion, as illustrated in the records of Fig. 3.

Although the eye rotation records are nominally independent of any translation motions of the eye, they are not completely independent over large translation motions. Moving the head laterally by ±0.5 mm, which would cause an eye movement artifact of approximately ±5° with a corneal tracker, can result in an artifact signal of several min of arc. Translation sensitivity to axial motion can be of similar size—several min of arc/mm of axial movement of the eye. With the eye relaxed to infinity, the optometer output can change by approximately 0.1–0.2 diopter/mm of head movement in any direction. The source of this residual translation sensitivity has not been completely explored, so it is not clear how much further this residual interaction can be reduced.

The sensitivity of the instrument in detecting translation motions is illustrated in Fig. 16. Part (a) of Fig. 16 illustrates axial eye motions recorded from the focus-detector diodes P_A and P_B of Fig. 4, with the focus servo inactivated. A simultaneous EKG recording, Fig. 16(b), verifies that the repetitive pattern is that of the heartbeat. Figure 16(c) shows a recording from the first Purkinje (horizontal) channel with the subject relaxed to infinity and voluntarily suppressing saccades. The heartbeat pattern does not show in the simultaneous fourth Purkinje record (not shown), indicating that the record is a pure translation motion of the eye (of approximately 30 μm), or a rotation component that is too small to see in the fourth Purkinje record. After vigorous exercise, both the rate and the amplitude of these eye translation motions increase, as shown in Fig. 16(d).

E. Eyetracker Overshoots

The eyetracker output often shows brief overshoots at the end of saccades [see the lower trace of Fig. 17(a)]. The source of these overshoots appears to be relative lateral motion of the lens within the globe, inasmuch as similar motions do not appear at all or are much smaller in the output from the first Purkinje tracker (i.e., in the motion of the first Purkinje image) [see the upper trace of Fig. 17(a)]. If this is the correct explanation, we might expect the size of the overshoots to vary with accommodation level (i.e., with changes in the physical configuration of the suspension of the eye lens). That this is the case can be seen from Figs. 17(b) and 17(c)

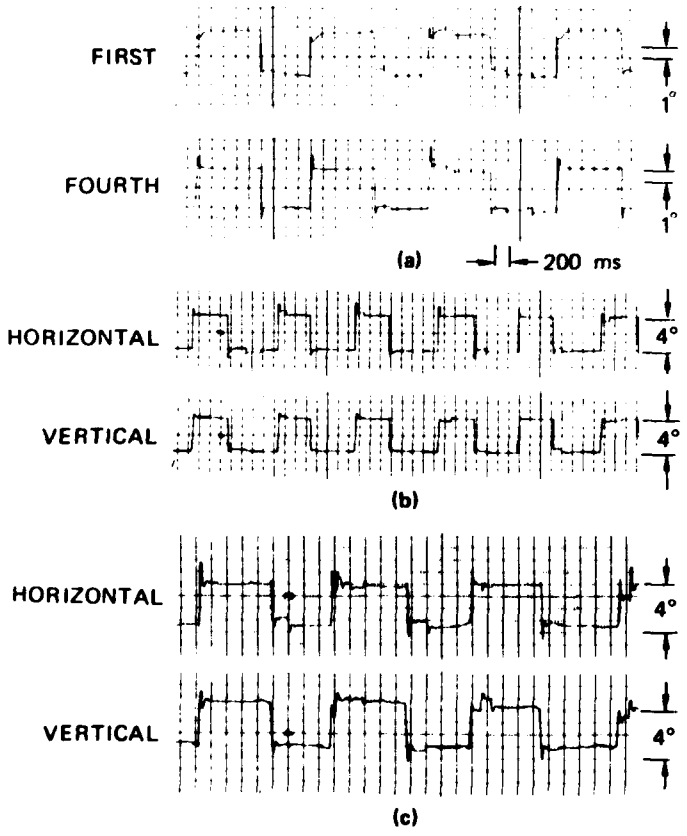

Fig. 17. Overshoots in the eye-movement records during saccades. As discussed in the text, these seem to be caused by lateral motions of the eye lens within the globe. (a) Simultaneous records from the first and fourth Purkinje image tracking systems. Note the small overshoots in the first Purkinje record and the large (and inconsistent) overshoots in the fourth Purkinje record. The 100–200-msec drift in the first Purkinje record, following each saccade, may be caused by a translation motion of the eye, inasmuch as a similar component is not seen in the fourth Purkinje record; (b),(c) comparing simultaneous horizontal and vertical overshoot components in the fourth Purkinje records with the subject relaxed to infinity and accommodated to 4 diopters. Note the large increase in overshoots at 4 diopters.

which shows the horizontal and vertical eye movement response to a diagonal target movement having 4° peak-to-peak components. In Fig. 17(b), the eye was relaxed to infinity, and in Fig. 17(c), the eye was accommodated to 4 diopters. At 4 diopters of accommodation, the limit for this subject, there is a large increase in the size and time constant of the overshoots in both the horizontal and vertical channels, as compared with relaxed accommodation. Still larger overshoots have been seen in subjects with larger accommodation. Note that the overshoots are not consistent from saccade to saccade, adding to the evidence that the overshoots are not in the instrument servoes. Also, the overshoots are generally larger in the horizontal than in the vertical direction for this subject.

If these overshoots derive from lateral motion of the lens within the globe, they provide a potentially useful method of measuring this motion. Also, such a motion causes a shift in the visual axis of the eye and, therefore, a shift in the retinal image. A large shift can have significant effects, for example, on the quality of image stabilization. We have estimated that the overshoots in the fourth Purkinje record are approximately ten times as large as the resulting shift in the visual axis, that is, a lateral shift of the lens large enough to cause a 1° overshoot in the fourth Purkinje record would actually represent about a 6-min shift in the visual axis of the eye.

If the magnitude of the overshoot could be scaled properly, the tracker would have an advantage in image stabilization over contact lens methods, which are insensitive to internal movements of the lens within the globe.

The stabilized image experiments referred to earlier[8] were performed without compensating for these overshoots, implying that even better image stabilization might result from proper compensation of the overshoot signals to make them correspond to the actual image displacement.

F. Binocular Records

Figure 18 shows simultaneous 3-D recordings of both eyes. During this record, both eyes were stimulated by square wave accommodation stimuli of 2 diopters. The accommodation responses are shown in the records labeled A_L and A_R. During period A, both eyes saw a target that was stationary except for a change in optical distance, and the eyes were nominally stationary (that is, the accommodation response was not accompanied by the usual vergence response). During period B, the left eye was occluded; recordings then showed the familiar vergence movement in response to the accommodation change. The lower trace, labeled $H_R - H_L$, is the difference between the left and right horizontal channels and therefore measures vergence. During period C, both eyes again saw a fixed target.

During periods D and F, the targets in both eyes were made to move in a sinusoidal pattern horizontally and sawtooth pattern vertically. Note that the records during these periods are similar to those of Fig. 13, except that both eyes are recorded simultaneously. During period E, the left eye was again occluded, and the H_L channel shows that the left eye responds now with both the accommodation-driven vergence stimuli and the sine wave motion of the right (seeing) eye, driven by the yoked version response.

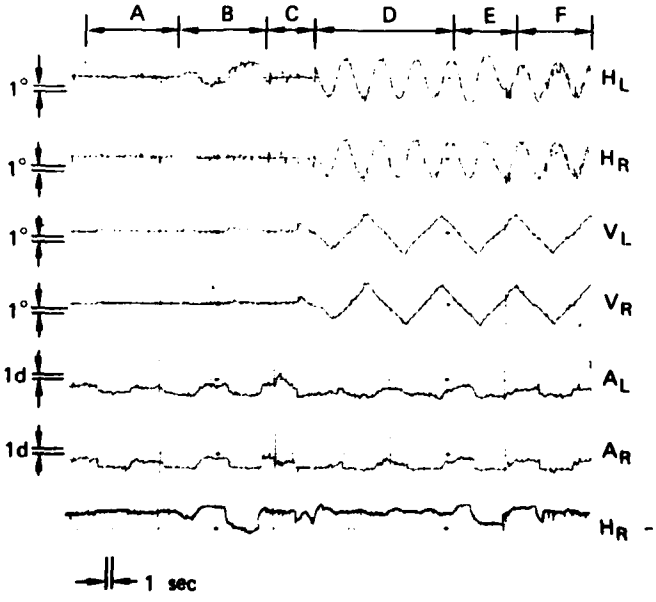

Fig. 18. 3-D, binocular record: H_L,H_R, horizontal motion in the left and right eye; V_L,V_R, vertical motion in left and right eye; A_L,A_R, accommodation in left and right eye; $H_R - H_L$, difference in horizontal motions in the two eyes (i.e., vergence) (see text for details).

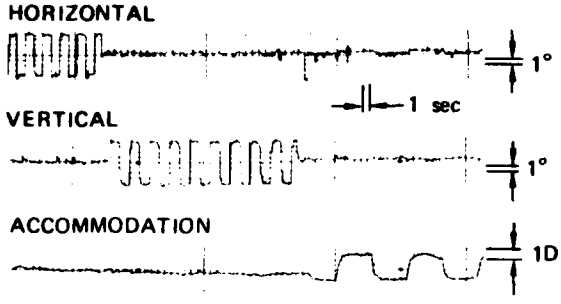

Fig. 19. Exploring channel interaction.

G. Channel Interaction

We have not yet studied in detail the effects of large eye movements on the calibration of the optometer and the effects of large accommodation changes on the calibration of the eyetracker. The records of Figs. 13 and 18 show that these effects are small, however, for ordinary eye movements and accommodation changes.

Nevertheless there are residual interactions. Figure 19 shows the 3-D response to a horizontal, then vertical, and then accommodation square-wave stimulus. There is almost no cross coupling into the other channels during the first two responses, although there is some coupling into the horizontal channel during the accommodation response. We do not yet know for sure how much of this coupling is in the eyetracker and/or stimulator and how much is in the eye, because there is some variation in cross coupling effects from subject to subject and even with the same subject from one session to another.

VII. Discussion

This instrumentation is relatively complex and operates on extremely low signal levels (especially the signals from the fourth Purkinje image of the 2-D eyetracker and from the retina in the optometer). Merging the two instruments, to achieve a 3-D tracker, required optical and electronic isolation measures so that the instruments would not interfere with each other. Furthermore, the latest version of the instrument is designed to tolerate head movements within 1 cm^3 of space. This required developing a method of translating the input light beams (without any rotation components) and an automatic focus system (without any accompanying change in magnification), as discussed in connection with Fig. 4. The resulting 3-D instrument has high accuracy and good frequency response in all channels although there is a small amount of channel interaction—especially between horizontal eye movements and accommodation. There is also a very small amount of translation artifact present in the eye rotation records. With further study and evolution, we hope to be able to define the ultimate limits of this visual tracking technique.

VIII. Summary

We have described a 3-D eyetracker that simultaneously tracks the horizontal and vertical movements of the eye as well as its instantaneous refractive power. The instrument is a synthesis of two previously described instruments: a double-Purkinje-image eyetracker and an optometer. The light sources for both instruments are near ir (0.93 μm) and are invisible to the subject. The eyetracker has a frequency response flat to approximately 300 Hz and operates over a field of more than 20° in diameter. The noise level of the eye-movement records is approximately 1 min of arc. Good stabilized-image disappearance has been achieved by moving the stimulus with the eyetracker output signals, which provides an indication of the accuracy and dynamic response of the instrument. The optometer operates over a range of 16 diopters with a noise level on the order of 0.1 diopter.

The instrument is easy to use; most new subjects can be aligned within a few minutes, and, once aligned, no adjustments are required as the subject moves in and out of the instrument. The instrument is designed to tolerate variations in head position within 1 cm^3; signals indicating the 3-D position of the eye are also available.

A pair of 3-D eyetrackers, combined with a pair of 3-D visual stimulators, form the basis of a binocular system in which each eye can be stimulated in X, Y, and focus independently, while the 3-D eye movements are recorded simultaneously from both eyes.

The detailed optical design of the second-generation eyetracker portion of the 3-D instrument was mainly the work of R. E. Savoie. The authors are indebted to Michael Clark for his general help in the later stages of the development and in obtaining the records described in the section on performance.

The work of merging the optometer and the improved double-Purkinje-image eyetracker was supported by NIH grant EY 01031 from the Department of Health, Education, and Welfare.

References

1. T. N. Cornsweet and H. D. Crane, J. Opt. Soc. Am. **60**, 548 (1970).
2. T. N. Cornsweet and H. D. Crane, J. Opt. Soc. Am. **63**, 921 (1973).
3. It is important to understand that the fourth Purkinje system tracks the position of the fourth image relative to the first. Thus, although we may sometimes refer simply to the fourth Purkinje output, what is meant is the position of the fourth image with respect to, or relative to, the first.
4. In the first-generation instrument, the 90° reflection at mirror M_1 in Fig. 2, caused coupling of vertical eye motions into the horizontal measurement channel. With a vertical eye movement, mirror M_1 rotates around axis aa (see inset in Fig. 2) to keep the first Purkinje image fixed on photocell P_1. This movement causes a rotation of the optical field around the first Purkinje image, producing artifactural change in the horizontal output for large eye movements. This problem is avoided in the new instrument by the 180° reflection at mirror M_{10}.

5. Experience with the first generation eyetracker showed that a center pivoted, 2-D mirror system is more accurate than a system that actually moves a photocell in two dimensions (i.e., photocell P_4 in Fig. 2). The new eyetracker therefore has two similar, 2-D servodriven mirror systems.
6. Isolation between instruments would be improved further if optometer light sources S_2 and S_3 emitted light of a different wavelength from that of eyetracker light source S_1. The two instruments could then be isolated by optical filters. Light emitting diodes of different wavelengths bright enough for this application are just now becoming available.
7. H. D. Crane and M. Clark, this same issue.
8. D. H. Kelly, "New Method of Stabilizing Retinal Images," at annual meeting of Opt. Soc. Am., Boston, 21–24 October 1975.

Appendix B

THREE-DIMENSIONAL VISUAL STIMULUS DEFLECTOR

Reprinted from Applied Optics, Vol. 17, No. 5, pp. 706-714 (1 March 1978)

Reprinted from APPLIED OPTICS, Vol. 17, page 706, March 1, 1978

Three-dimensional visual stimulus deflector

H. D. Crane and Michael R. Clark

A 3-D visual stimulus deflector has been designed so that a subject can view any stimulus pattern or object through it, and the pattern (up to 25° in diameter) can be moved over a range of 40° horizontally and 30° vertically. The optical distance of the object being viewed can be changed over a 15-diopter range, while the brightness and visual angle subtended by the object remain fixed. Further, the observer can view the object through a pupil of any desired shape and transmittance. Horizontal and vertical movements are independent, with time delays of 1 msec and a response range from dc to 200 Hz. Focus change is independent of lateral field motion and has a time delay of 12 msec and a maximum slewing rate of approximately 40 diopters/sec. Two such devices can be aligned side by side in a binocular configuration for independent 3-D control of the fixation of each eye.

I. Introduction

To test the human visual system in a clinical or research setting, it is often necessary to move a target in specific ways to stimulate certain types of eye movements in the subject (patient). The instrument described here can move the visual stimulus horizontally and vertically, as well as stimulate accommodation (focus) by altering the optical distance of the target from the subject. The subject views the target through the deflector. Horizontal and vertical movements and focus change are accomplished with three independent servosystems. Independent, 3-D stimulation of both eyes is achieved by two devices aligned side by side.

The basic principle of operation may be summarized as follows (see Fig. 1). The subject's eye is positioned in front of the first lens pair LP_1 so that the center of rotation CR of the eye is imaged on the axis of rotation of mirror M_V. The two lenses of LP_1 are identical and separated by the sum of their focal lengths. This pair of identical lenses separated by the sum of their focal lengths produces an undistorted unity-magnification image. Mirror M_1 is fixed in position; mirror M_V is rotated by a closed-loop servomotor system to produce vertical movement of the visual field.

The eye is imaged a second time by lens pair LP_2. Mirror M_H is positioned so that the eye's center of rotation in the second image falls on the axis of mirror M_H. Mirror M_H is rotated by a second closed-loop servomotor system to produce horizontal movement of the visual field. With the axes of rotation of both mirrors conjugate to CR, pure horizontal and vertical movement of the visual field is achieved without either translation effects or image size changes.

The plane of the eye's pupil is conjugate to a plane labeled AP (artificial pupil). If a stop smaller than the natural pupil is placed in the artificial pupil plane, it becomes the limiting aperture of the system; consequently, the effects of natural pupil changes are eliminated. Cylindrical and spherical correction lenses for each subject can be placed in a trial lens holder located in front of aperture AP. Since plane AP is conjugate with the pupil of the eye, correction lenses placed near plane AP should have the same visual effect as if they were placed directly at the spectacle plane.

The second lens pair, LP_2 is positioned so that its first lens L_3 is located one focal distance from plane AP. Simultaneous axial movement of lens L_4, mirror M_H (with its servomotor), and mirror M_2 adjusts the spherical power of the system without change in image position, size, or brightness. As we will show, spherical power, in diopters, is linearly related to the axial position of the movable carriage, which can be adjusted manually or driven by a third servomotor. Lenses L_1, L_2, L_3, and L_4 are actually multiple-element camera lenses.

II. Theory of Operation

To understand the optics of the system, a discussion of certain properties of a pair of lenses separated by the sum of their focal lengths is necessary. The configuration used may be regarded as a relay-lens system.

The authors are with Stanford Research Institute, Menlo Park, California 94025.

Received 2 July 1977.
0003-6935/78/0301-0706$0.50/0.

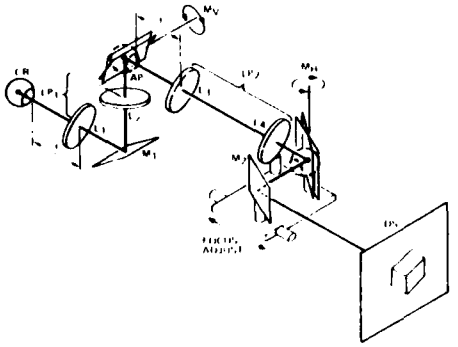

Fig. 1. Schematic diagram of the 3-D visual stimulator. *CR*, center of rotation of eye; L_1, L_2, L_3, and L_4, multiple-element camera lenses; *LP*, lens pair; *AP*, artificial pupil; *DS*, display screen; M_V, mirror that rotates the visual field vertically; M_H, mirror that rotates the visual field horizontally; M_1, fixed mirror; L_4, M_H, and mirror M_2 move in synchronism to adjust the optical distance to the display screen (see Fig. 8).

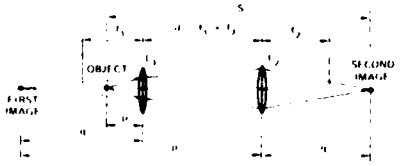

Fig. 2. Two-lens system. f_1, f_2, focal lengths of lenses L_1, L_2; p, object distance to L_1; q, first image distance from L_1; p', object distance from L_2; q', second-image distance from L_2; d, separation between L_1 and L_2; S, separation between object and second image.

A. Linear Object–Image Motion

Figure 2 illustrates a pair of positive lenses of focal length f_1 and f_2, separated by a distance d. An object at distance p from the first lens ($p < f_1$) forms an image at distance q' from the second lens.

It is well known that if $p = f_1$ then $q' = f_2$, independent of the separation d, and there is an image magnification $M = f_2/f_1$. Less well known is that when $d = f_1 + f_2$ (i.e., when the lenses are separated by the sum of their focal lengths), the distance p and q' are linearly related, and magnification M is independent of p.

For $p < f_1$ the image formed by L_1, labeled the first image in Fig. 2, will be virtual and located at a distance

$$q = -pf_1/(p - f_1) \tag{1}$$

on the same side of the lens as the object. This first image is at a distance

$$p' = q + (f_1 + f_2) = \frac{pf_2 - f_1(f_1 + f_2)}{p - f_1} \tag{2}$$

from the second lens and forms a second image at a distance

$$q' = \frac{p'f_2}{p' - f_2} \tag{3}$$

from the second lens. Substituting Eq. (2) into Eq. (3) produces

$$q' = \left[f_2\left(1 + \frac{f_2}{f_1}\right)\right] - \left(\frac{f_2}{f_1}\right)^2 p. \tag{4}$$

Thus the image distance q' is linearly related to the object distance p through the constant factor $(f_2/f_1)^2$. With $p = f_1$, Eq. (4) reduces to $q' = f_2$. It is straightforward to show that the same results are true for $p > f_1$.

The magnitude of the lateral magnification M between the object and final image can be determined from

$$M = \left|\frac{q}{p}\cdot\frac{q'}{p'}\right| = \left|\frac{-pf_1/(p - f_1)}{p}\cdot\frac{p'f_2/(p' - f_2)}{p'}\right| \tag{5}$$

or

$$M = \left|\frac{-f_1f_2}{(p - f_1)(p' - f_2)}\right|. \tag{6}$$

Substituting Eq. (2) for p' results in the simple equation

$$M = f_2/f_1, \tag{7}$$

which depends only on the ratio of the focal lengths and is independent of p.

Because axial image position is linearly related to object position and lateral image magnification is independent of object distance, axial magnification is uniform, and lateral magnification is constant in the image [see Fig. 3(a) for the case of $f_2/f_1 = 2$]. In this case, lateral magnification is two, and axial distances are scaled by $2^2 = 4$. Figure 3(b) shows the usual distortion that results from single lens imaging for the same magnification.

B. Object–Image Separation

The separation S between the object and the second image in Fig. 2 is

$$S = p + (f_1 + f_2) + q' \tag{8}$$

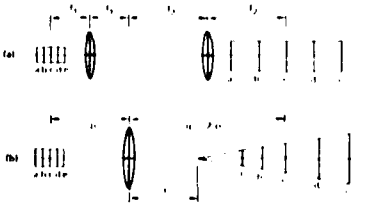

Fig. 3. (a) Relay lens pair. Lateral and axial magnification are independent of axial position of the object. Note the distortionless and constant imaging from (*abcde*) to (*a'b'c'd'e'*). (b) Typical distortion of single-lens imaging.

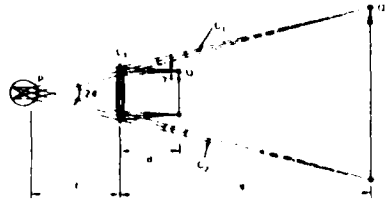

Fig. 4. Schematic representation of a simple Badel optometer. The pupil plane of the eye is placed one focal length f from lens L_1; the object, a distance d from L_1, subtends a visual angle 2θ; a virtual image of the object is formed at a distance g from L_1; note the backward projection of central rays C_1 and C_2; p, pupil diameter.

Substituting Eq. (4) for q' results in

$$S = p\left[1 - \left(\frac{f_2}{f_1}\right)^2\right] + f_1\left(1 + \frac{f_2}{f_1}\right)^2. \tag{9}$$

For $p = f_1$, Eq. (9) reduces to $2(f_1 + f_2)$. For $f_1 = f_2 = f$, the separation is constant and equal to

$$S = 4f, \tag{10}$$

independent of p. This result is expected once it is noted that, with equal-power lenses, image movement exactly tracks object movement. Alternatively, for a fixed object location, the lens pair itself can be moved without affecting the image position.

Even if there is a nonunity ratio, magnification will still remain constant although S varies linearly with p. Thus, if the spacing between the object plane and the desired image plane should change, either because the object moved or because the image screen moved, the system can be refocused by moving the lens pair along the optic axis. When refocused, the image will be unchanged in size because of the constant magnification property.

C. Basic Principle of Focus Corrector/Deflector

In the optical system sometimes referred to as a Badel optometer, the eye views an object through a lens that is located one focal length from the pupil of the eye, as illustrated in Fig. 4. (More specifically, the lens is placed one focal length from the first nodal point of the eye, which is approximately in the pupil plane of the eye.) The optical power of the system is adjusted by varying the distance d between the object and lens. Lens L_3 of Fig. 1, which is located one focal length from the first image of the pupil, is functionally equivalent to lens L_1 of Fig. 4. Movement of lens L_4 in Fig. 1 varies the distance d between the real image formed of the display screen DS and lens L_3. Hence, L_3 functions as a Badel optometer that is separated from the eye by a relay lens pair LP_1.

Viewing through lens L_1 of Fig. 4, the eye sees the object, located a distance d on the far side of the lens, imaged at a distance $f + g$ from the lens. As illustrated by Fig. 4,

$$1/g = 1/d - 1/f \tag{11}$$

or

$$g = (fd)/(f - d), \tag{12}$$

and therefore

$$f + g = f^2/(f - d). \tag{13}$$

The distance to the image in diopters D_E is

$$D_E = \frac{1}{f + g} = \frac{1}{f}\left(1 - \frac{d}{f}\right) = D_o\left(1 - \frac{d}{f}\right), \tag{14}$$

where f and g are measured in meters, and $D_0 = 1/f$ is the dioptric power of the lens. If $d = f$, the object appears at infinity, and the relative power of the eye D_E required to focus the object is zero.[1] If $d = 0$, the lens has no optical effect, and the object appears to the eye at the distance of the lens. The accommodation power required to focus it is therefore $1/f$, or D_o, diopters. If $d > f$, the object appears beyond infinity, and the required eye power is negative. Note that the relationship expressed in Eq. (14) between eye diopters and distance d is linear.

The angular size of the object is independent of d because the backward projection of the central rays from each point of the object, for example, rays C_1 and C_2 from the two extreme points of the object are independent of d. Image brightness is also independent of d because the fan of rays accepted from each point of the object is independent of d. To see this, note that the fan of rays accepted at the pupil from object point Q has an angular extent γ as viewed from the object point. Using the small angle approximation, we have

$$\gamma = \{pg/(f + g)\}/d, \tag{15}$$

where p is the pupil diameter. Substituting Eq. (12) and Eq. (13) into Eq. (15) results in

$$\gamma = p/f, \tag{16}$$

which is independent of d. This result is true for every point of the object. For this reason, image brightness is independent of the focal power of the instrument.

Crane and Cornsweet devised a system, shown in Fig. 5, that does not require the object to be moved to change the virtual distance d.[2] An image of the object to be viewed is formed by a lens L_2 in the space between L_1 and L_2. The distance from this real image to lens L_1 (distance d) is smoothly varied by means of a four-component mirror system. With the eye fixed in the focal plane of lens L_1, an image of the eye pupil is formed in the focal plane to the right of lens L_2. For this method of imaging, the light coming to focus at AP is collimated between the lenses, and the image of the eye pupil is therefore unaffected by movement of the mirrors. Hence, an artificial pupil AP can be used in this image plane.

D. Large Field of View

Using spherically corrected doublets, a system of the form shown in Fig. 5 can operate well over a viewing field up to about 10°. To increase the field of view, however, requires camera-quality optics.

To understand the optical requirements, let us sim-

Fig. 5. Crane and Cornsweet focus stimulator: *DS*, display screen; *AP*, artificial-pupil plane. Mirrors R_2 and R_3 are moved orthogonal to the optic axis to change the optical distance to *DS*.

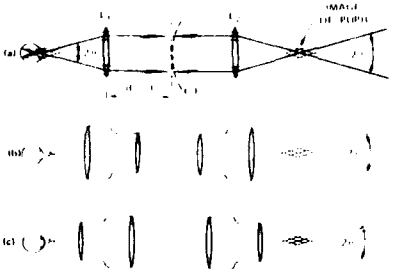

Fig. 6. (a) Schematic diagram of a relay lens pair with a visual field 2θ. The pupil plane of the eye is placed at the focal plane of L_1. Assume the eye is focused at infinity, i.e., $d = f$. C. F. depicts curvature of field. (b) Camera-quality lenses arranged for minimal blurring of images at the retina. (c) Camera-quality lenses arranged to minimize spherical aberration.

plify the drawing by straightening out the path between the lenses of Fig. 5, as shown in Fig. 6(a), in which the eye is shown focused for infinity, and the image of display screen *DS* is also at infinity, i.e., $d = f$. In effect, the eye views the target through the entrance pupil formed by lenses L_1 and L_2. There are two conflicting requirements for good imaging in this case. First, zero field distortion requires that the chief rays (shown dark in the figure) passing through the center of the real pupil should also intersect at the center of the pupil image. (In this case, the field angle, labeled 2θ, would be the same whether seen from the real pupil or from the pupil image.) This requires zero spherical aberration in the plane of the pupil. Second, note that a real image of the infinitely distant scene is formed in the plane between the two lenses. This real image serves, in turn, as the virtual object for lens L_1. Any curvature of field in this image plane, as suggested by curved line C.F. in the figure, would cause off-axis blurring of the image at the retina. These requirements—zero spherical aberration and flat-field imaging—generally conflict for doublet lenses.

Camera lenses substituted for lenses L_1 and L_2 should be arranged as shown in Fig. 6(b) to minimize blurring of the target at the retina. That is, they should be arranged as though the plane between the two lenses is the normal film plane; camera lenses are specifically designed for flat-field imaging in this direction. On the other hand, to minimize spherical aberration in imaging the eye pupil, the lenses should be reversed, as shown in Fig. 6(c). Recall that with respect to the pupil, the rays are collimated between the lenses. The design discussed here is based on a relatively symmetric 50-mm Olympus *f*/1.8 camera lens which can be used almost equally well in both directions, although configuration 6(c) provides a significantly wider field of view.

The difficulty with camera lenses, whether used in configuration 6(b) or 6(c), is that they are too large to use with the four-mirror scheme of Fig. 5. The only practical arrangement is to move the lens itself, as illustrated in Fig. 7(a). The disadvantage of moving the lens is that unless the display screen is at optical infinity, the distance from the screen to the lens is then variable, and the image formed between the lenses is no longer constant in size. The situation can be remedied with an extra fixed lens if the display screen can be placed directly in the focal plane of the extra lens. By using two extra lenses, L_3 and L_4 [as shown in Fig. 7(b), where L_4 generates a real image of the display screen in the focal plane of lens L_3], the system can then accommodate a continuous range of distances between the device and display screen. That is, for a given position of the display screen *DS*, lens L_4 is adjusted axially until image *DS′* is in the focal plane of lens L_3. This places the image *DS′* of *DS* at infinity, making the image size independent of focus adjustments.

Two extra lenses are necessary, in any case, for achieving two-axis visual deflection as well as focus control. That is, two separate images of the eye pupil

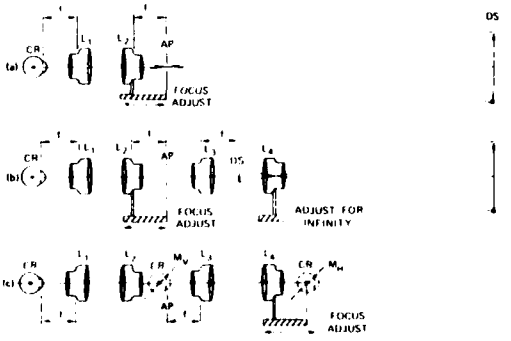

Fig. 7. (a) Simple focus stimulator. Lens L_2 moves axially to vary dioptric power; artificial pupil *AP* eliminates any effects caused by changes in the eye pupil; DS, display screen. (b) Focus stimulator that compensates for variable axial position of the display screen. L_4 is moved axially to create an image of *DS* in the focal plane of L_3, thereby ensuring that the target *DS* appears at optical infinity to the focus stimulator system (L_1, L_2). (c) Three-dimensional visual stimulator; M_V and M_H, rotating mirrors; *CR*, center of rotation of eye; *CR′*, *CR″*, first and second images of *CR*. With *CR′* and *CR″* on the axes of rotation of M_V and M_H, respectively, vertical and horizontal movement of the visual field is achieved without translation artifact.

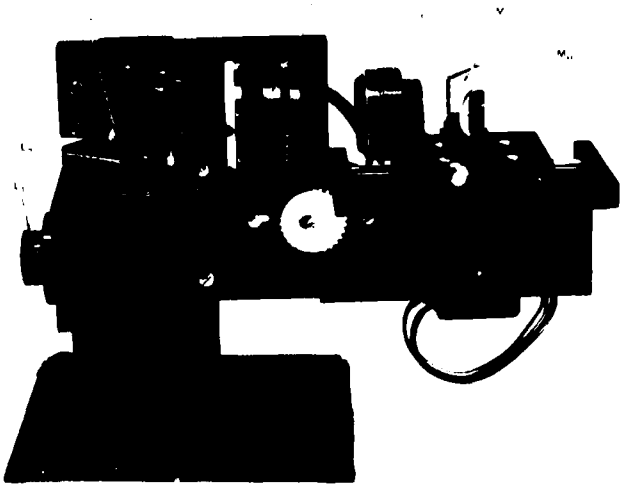

Fig. 8. Three-dimensional visual stimulator (see schematic diagram of Fig. 1).

are required as locations for two single-axis mirror deflectors, as illustrated in Fig. 1 and again in Fig. 7(c). Mirror M_V is positioned at the first image location (between the two lens pairs); mirror M_H is located at the second image location (beyond the second lens pair). It was noted earlier that to achieve pure rotation of the visual field without translation effects, it is necessary that the eye's center of rotation be conjugate to some point on the axis of rotation of each mirror. If lens L_2 were used for focus control, as shown in Fig. 7(b), both images of the eye's center of rotation would shift axially with respect to the mirror axes shown in Fig. 7(c), unless both servomotor mirror assemblies shifted axially by different amounts in synchronism with L_2. The system is greatly simplified if lens L_4 is used instead for focus adjustment, in which case only mirror assembly M_H must be moved axially, as shown in Fig. 7(c).

With the position of Lens L_4 adjustable, the spacing between lenses L_3 and L_4 is no longer constant, and the imaging of the eye at mirror M_H is no longer distortionless as it would be if the distance between L_3 and L_4 were equal to the sum of their focal lengths. But only small errors result. Appendices A, B, and C analyze the magnitude of the errors inherent in the system.

III. Performance

Figure 8 shows the 3-D visual stimulator. The field of view is approximately 25° in diameter. The center of the field can be moved through an angle subtending ±15° vertically and/or ±20° horizontally at the eye. The spherical power can be changed from −4 diopters to +11 diopters with a movement sensitivity of 2.5 mm/diopter. Each camera lens has ten surfaces. The loss of light when viewing through the forty coated surfaces of four camera lenses in series is equivalent approximately to a 0.3 neutral density filter.

The electronics that produce horizontal and vertical deflections consist of the two General Scanning CCX-101 amplifiers that drive the G300PD Optical Scanners (see Fig. 9). The scanners have angular rotation sensors that are used to derive angle and angle rate signals that are part of a servo loop. A readout of the angular position of the scanners is available. Gain and offset controls condition the input signal while loop gain and damping adjustments are also available.

The deflection servosystems are capable of rotating the mirrors by more than 25° (50° movement of the visual target) with a linearity of ±0.1% of the excursion. The resolution is approximately 10 sec of arc with a response from dc to 3-dB bandwidth of 200 Hz. The delay time (0–10%) is less than 1.5 msec, and the 10–90 risetime is less than 2.5 msec. The total response time is approximately 6 msec .

The focus servo, a closed-loop system with position feedback, is capable of changing spherical power by more than 14 diopters with a sensitivity of approximately 9 diopter/V. The linearity is ±0.25% of the peak-to-peak range with a repeatability of less than 0.1 diopters. The time delay to a step is 12 msec with a maximum slewing rate of 40 diopter/sec.

IV. Summary

A 3-D visual stimulus deflector consists of four identical camera lenses in series. It is shown that a pair of identical lenses separated by the sum of their focal lengths generates an undistorted 3-D image independent of the distance that the object is from the lens pair. With two such pairs of lenses, two undistorted images are created, one in the space between the second and third lens and one in the focal plane beyond the fourth lens. The eye sees the world as though viewing through this second image of itself. A rotatable mirror is located at each of these image positions and adjusted so that the image of the eye's center of rotation falls on each axis of rotation. In this case, the field of view seen by the eye can be moved as though with a pure eye rotation, that is, without translational effects. A mirror that rotates about a horizontal axis is located at the first image position, and a mirror that rotates about a vertical axis is located at the second image position. These mirrors move the visual world in a vertical and horizontal direction.

Focus change is achieved by moving the fourth lens and second mirror in synchronism along the optical axis of the device. Although such movement alters the spacing between the third and fourth lenses (so they no

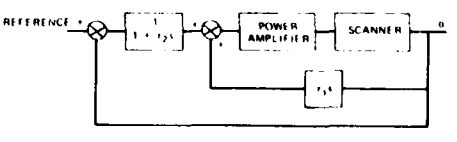

Fig. 9. Schematic diagram of deflection servoloop electronics.

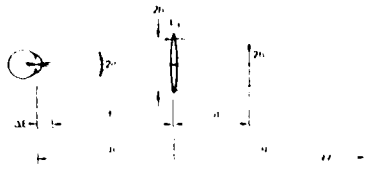

Fig. 10. Diagram of the change in visual angle as a function of object distance d from lens L_1 and axial misalignment of the eye by distance ΔE from the focal plane of L_1.

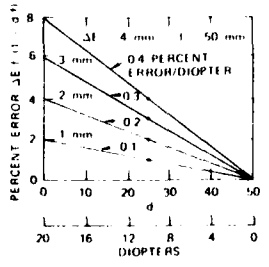

Fig. 11. Percent error in the visual angle θ as a function of the distance d of the object from lens $L_1(f = 50$ mm).

longer form a distortionless imaging system) the errors thereby induced are small (see Appendices).

The instrument is built around four 50-mm $f/1.8$ camera lenses. It can move a visual stimulus 25° in diameter over a range of 40° horizontally and 30° vertically. The optical focus of the object being viewed can be changed over a 15-diopter range, while the brightness and visual angle subtended by the object remain invariant. Movement of the two mirrors and the axial movement of the last lens and second mirror system are controlled by three independent servosystems.

Appendix A

It was stated in the body of the paper in connection with Fig. 4 that if the eye is located in the focal plane of lens L_1, the image size is independent of distance d. Let us inquire how sensitive this constancy is to the axial position of the eye.

Assume the eye is moved a distance ΔE from the focal plane, that is, the eye is at a distance $f + \Delta E$ from lens L_1, and that the eye pupil is stopped down to a pinhole. In this case, the rays accepted from each point of the object will no longer be parallel, as shown in Fig. 4, but will converge as shown in Fig. 10. These accepted rays intersect at a distance q from the lens, where p and q can be thought of as object and image distances, that is,

$$q = \frac{pf}{p - f} = f\left(\frac{f + \Delta E}{\Delta E}\right). \tag{A1}$$

The height $2h'$ of the accepted ray bundle at the lens can be written as

$$2h' = \frac{q}{q - d} \cdot 2h = \frac{1}{1 - (d/q)} \cdot 2h, \tag{A2}$$

where $2h$ is the object size. The angular size of the object, as seen from the eye, is

$$2\theta \sim (2h')/(f + \Delta E), \tag{A3}$$

where the small-angle approximation is made that the angle is equal to its tangent. Substituting Eqs. (A1) and (A2) into Eq. (A3) gives the equation

$$\theta = \frac{h/f}{1 + \frac{\Delta E}{f}\left(1 - \frac{d}{f}\right)} \tag{A4}$$

$$\approx \theta_0\left[1 - \frac{\Delta E}{f}\left(1 - \frac{d}{f}\right)\right], \tag{A5}$$

where the half angle $\theta_0 = h/f$.

Note that $\theta = \theta_0$ either if $\Delta E = 0$ (i.e., if the eye is in the focal plane) or if $d = f$ (i.e., if the object being viewed is at infinity). If $\Delta E \neq 0$, the image size will change as the object distance d changes. Figure 11 is a plot of the error factor $(\Delta E/f)\,[1 - (d/f)]$ for a 50-mm (20-diopter) lens. Note that according to Eq. (14) the eye will experience a 20-diopter change when the object shifts from $d = f$ to $d = 0$ (i.e., for a movement equal to f). The diopter change per millimeter of object movement can therefore be written

$$S = \frac{f}{1000/f} = \frac{f^2}{1000}\ \text{mm/diopter} \tag{A6}$$

or 2.5 mm/diopter for a 50-mm lens.

From Fig. 11, we see that with the eye displaced 2 mm axially, there is a 1% change in image size for a 6-diopter change (i.e., for a movement from $d = 50$ mm to $d = 35.0$ mm).

If the device is used as an ocular corrector, it is not important that the eye be in the exact axial plane because the target distance will not be changed. If the device is to stimulate focus change with constant image

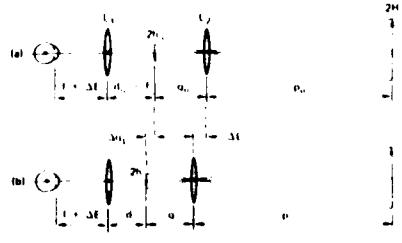

Fig. 12. Schematic representation of the axial shift Δq_L of an image because of a shift ΔL of L_2. The eye is at a distance $f + \Delta E$ from L_1. (a) Before lens movement, the object, height $2H$, is at a distance p_o from L_2 and forms an image of height $2h_o$ at distance q_o from L_2 and $d_o = f$ from L_1. (b) After lens movement ΔL, the object is at distance $p = p_o + \Delta L$ from L_2, and the image, height $2h$, is shifted by Δq_L to distance q from L_2 and d from L_1.

size, however, alignment is important. The simplest way to adjust axial eye position is to move the eye axially slowly while the target shifts back and forth, until the subject reports no size change associated with the focus change. If the eye is too close to (or too far from) the lens, the target will increase (or decrease) in size as the target is brought toward the lens—i.e., decreasing d.

Appendix B

Figure 7 illustrates an axial lens shift to vary the focus. As we saw, however, unless the target is at infinity, this axial movement will cause a change in the size of the image. Also, the image will not move exactly the same amount as the lens movement. For the purpose of the following analysis, let Δq_L be the amount the image moves in response to a lens movement ΔL. The situation is shown in Fig. 12, where a deliberate axial shift of the eye is used to compensate for this variation in image size. In other words, focus change can be achieved while maintaining constant image size even with the target not at optical infinity. To obtain this result, we must find a value of ΔE such that θ (image size) is independent of d (distance).

Equation (A4) shows the general relation between θ,h, ΔE, and d, where the size of the real image being viewed $2h$ is now a variable. We will derive general relations for h and d as functions of ΔL.

By differentiating the general lens equation,

$$q = (pf)/(p - f), \tag{B1}$$

with respect to p, we find that for a small change Δp in object distance (lens fixed in position), the corresponding change in q is

$$\Delta q = -(q^2/p^2)\Delta p. \tag{B2}$$

If the object distance change is because of a shift ΔL in the lens, however, rather than because of a change in object position, the corresponding change in image position is simply equal to Δq plus the amount of the lens movement, i.e.,

$$\Delta q_L = \Delta L + \Delta q. \tag{B3}$$

Substituting Eq. (B2) into Eq. (B3) and noting that $\Delta p = \Delta L$, we obtain

$$\Delta q_L = \Delta L[1 - (q/p)^2]. \tag{B4}$$

In other words, if the lens moves by an amount ΔL to the left, the distance d decreases to

$$d = d_o - \Delta q_L \tag{B5}$$

$$= d_o - \Delta L[1 - (q/p)^2]. \tag{B6}$$

Let us consider next how image size varies with ΔL. The ratio of image size to object size is directly related to the ratio q/p, that is,

$$2h = (q/p) \cdot 2H, \tag{B7}$$

where q and p can be expressed as

$$p = p_o + \Delta p, \tag{B8}$$

$$q = q_o + \Delta q = q_o - (q/p)^2\Delta p. \tag{B9}$$

Substituting Eqs. (B8) and (B9) into Eq. (B7), we obtain

$$h = h_o \frac{1 - \left[\left(\frac{q}{p}\right)^2 \cdot \frac{\Delta p}{q_o}\right]}{1 + \frac{\Delta p}{p_o}}, \tag{B10}$$

where $h_o = (q_o/p_o)H$. Ignoring second-order terms, Eq. (B10) becomes

$$h \approx h_o\left[1 - \frac{\Delta L}{p_o}\left(1 + \frac{q_o}{p_o}\right)\right], \tag{B11}$$

where ΔL is substituted for Δp. Substituting Eqs. (B6) and (B11) into Eq. (A4) and ignoring the subscripts on p, q, and d, we obtain

$$\theta \approx \frac{h_o}{f\left[1 + \frac{\Delta E}{f^2}(f - d)\right]} \cdot \frac{1 - \frac{\Delta L}{p}\left(1 + \frac{q}{p}\right)}{1 + \frac{\Delta E \Delta L\left(1 - \frac{q^2}{p^2}\right)}{f^2 + \Delta E(f - d)}}. \tag{B12}$$

Note that if the last terms of both the numerator and denominator are equal, Eq. (B12) reduces to

$$\theta \approx \frac{h_o}{f} \cdot \frac{1}{1 + |(\Delta E)/(f^2)|(f - d)}, \tag{B13}$$

and θ is independent of ΔL, which is what we wished to demonstrate. The equality of numerator and denominator in Eq. (B12) requires that

$$\Delta E = \frac{-f^2}{(p - q) + (f - d)}. \tag{B14}$$

Figure 13 is a plot of Eq. (B14) for $f = d$, i.e., where the target appears to be at infinity, and therefore defines the initial ΔE for most experimental conditions. Note that ΔE is negative because as lens L_2 moves toward lens L_1, the image decreases in size. To compensate for this decrease, the eye must be moved closer to lens L_1. For example, for an object 1 m away (p = 1000 mm), the

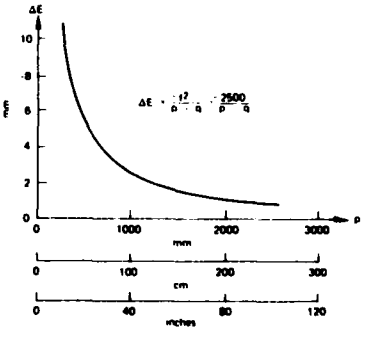

Fig. 13. Plot of ΔE as a function of the object distance p (from L_2) necessary to produce constant size imaging by lens system L_1, L_2 in Fig. 12. Note that $f = d$.

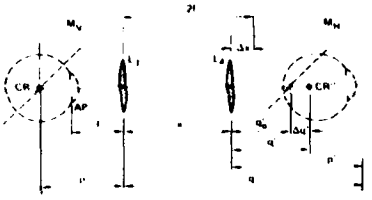

Fig. 14. Diagram of the axial movement $\Delta q'$ of the second image CR'' of the eye's center of rotation CR as a function of (L_4, M_H) movement by amount Δx. Before movement, Δx is zero and $x = 2f$; CR'' is at a distance q_o from L_4 and falls on the axis of rotation of M_H. After movement, CR'' is displaced by $\Delta q'$ from the axis of rotation of M_H. The first image CR' of CR is formed at the axis of rotation of M_V, which is at a fixed distance p from L_3. An image of CR' is formed at distance q' from L_4.

eye must be moved approximately 2.5 mm closer to L_1. Note that there is a very small sensitivity to the exact slide position before it is moved. For example, for $p = 1000$ mm, there is approximately a 1.3% change in ΔE for $d_0 = f$ (the slide at the infinity position) or for $d_0 = \frac{3}{4}f$ (the slide at the 5-diopter position).

Appendix C

Even if mirror M_H moves in synchronism with lens L_4, as illustrated in Fig. 7(c), the second image CR'' of the eye's center of rotation moves away from the surface of mirror M_H as lens L_4 moves over its range, as shown in Fig. 14. Therefore, rotation of M_H will not be perceived as pure rotation by the eye. The following discussion quantifies the expected variation of the translation component thereby induced.

Figure 14 depicts the geometry of interest. CR', the image of CR formed at M_V, is at a distance p from L_3.[3] Its image distance q may be written

$$q = (pf)/(p - f). \tag{C1}$$

The object distance p' for lens L_4 can be written

$$p' = x - q = x - [(pf)/(p - f)] \leq 0, \tag{C2}$$

where x is the separation between lenses L_3 and L_4. The separation x can in turn be written as

$$x = 2f + \Delta x, \tag{C3}$$

where Δx (positive or negative) represents the simultaneous movement of L_4 and M_H, as shown in Fig. 7(c). Substituting Eqs. (C1) and (C3) into Eq. (C2), we have

$$p' = \frac{pf - 2f^2}{p - f} + \Delta x. \tag{C4}$$

For simplicity, if we assume $p = kf$, $k > 1$, then Eq. (C4) becomes

$$p' = [(k - 2)/(k - 1)]f + \Delta x. \tag{C5}$$

The final image distance q' is

$$q' = \frac{p'f}{p' - f} = \frac{[(k - 2)/(k - 1)]f^2 + (\Delta x)f}{[(-f)/(k - 1)] + \Delta x}. \tag{C6}$$

Dividing the numerator by the denominator, we have

$$q' = f + (1 - k)f \Big/ \left[1 - \frac{(k - 1)}{f}\Delta x\right]$$

$$\approx f + [(1 - k)f]\left[1 + \frac{(k - 1)}{f}\Delta x\right]$$

$$\approx (2 - k)f - (k - 1)^2\Delta x. \tag{C7}$$

Writing q' in the form

$$q' = q_o' + \Delta q' = q_o'\left(1 + \frac{\Delta q'}{q_o'}\right) \tag{C8}$$

and substituting Eq. (C7) into Eq. (C8), we have

$$q_o' = (2 - k)f, \tag{C9}$$

$$\frac{\Delta q'}{q_o'} = -\frac{(k - 1)^2}{2 - k} \cdot \frac{\Delta x}{f}. \tag{C10}$$

Figure 15 is a plot of $|\Delta q')/(q_o')|$ as a function of $(\Delta x)/f$, assuming $k = 1.2$. The maximum variation is 2.5% of q_o' in the worst case. This error will cause the conjugate image of the center of rotation to be displaced by this amount from the axis of the rotating mirror M_H. Consequently, the rotation of the eye caused by a given angular rotation of the mirror will not be exactly the same as the mirror rotation, or conversely, the rotation of the mirror necessary to compensate a given eye rotation will not be exactly the same size as the eye rotation.

The rotational error is depicted in highly exaggerated form in Fig. 16, where for simplicity the target is shown along the axis rather than as deflected by mirror M_H (i.e., as though M_H were not there). If M_H caused the

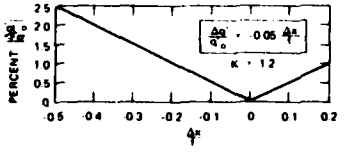

Fig. 15. Percent error $|(\Delta q')/(q_o')|$ as function of the change in axial separation $(\Delta x)/f$ of L_3, L_4.

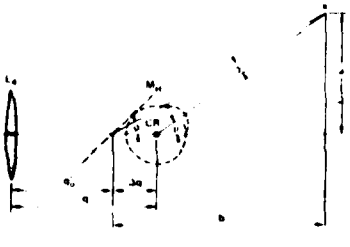

Fig. 16. Schematic diagram of the difference between rotational angle ϕ and visual angle θ, where the target is at a distance b from the axis of rotation of M_H and where the axis of rotation of M_H and CR'' are separated by a distance $\Delta q'$.

target to be rotated through an angle ϕ, the eye must rotate through an angle θ, where ϕ and θ differ by an amount

$$\gamma = \theta - \phi \tag{C11}$$

because of the offset $\Delta q'$. These angles can be written as

$$\phi = \tan^{-1}(a/b), \tag{C12}$$

$$\theta = \tan^{-1}|a/(b - \Delta q')|, \tag{C13}$$

where b is the target distance from the axis of the mirror, which is approximately 1 cm larger than the distance from (the image of) the pupil to the target. For the present applications,

$$\phi \leq 10° \tag{C14}$$

and

$$b > 10 \text{ cm } (D_E < 10 \text{ diopters}). \tag{C15}$$

Therefore,

$$a \leq b \tan 10° = 0.176b. \tag{C16}$$

From Eqs. (C9) and (C10), it can be noted that

$$|\Delta q'| = (k - 1)^2 \Delta x. \tag{C17}$$

In the present design, $k = 1.2$ and $\Delta x \leq f/2$. Given $f = 50$ mm, then $b > 2f = 10$ cm. When we combine these relationships, Eq. (C17) becomes

$$|\Delta q'| = 0.04\Delta x \leq 0.02f \leq 0.01b, \tag{C18}$$

$$\theta \leq \tan^{-1}(0.176/0.99) = 10.1°, \tag{C19}$$

$$\gamma = \theta - \phi \leq 0.1°. \tag{C20}$$

Thus, in the worst case, there is an (0.1/10) or 1% error between actual eye rotation and rotation of M_H because of the movement of lens L_4.

If ϕ and the dioptric power $[D_E = (1/b)]$ are constant, the gain of the servo driving M_H can be changed to overcome this artifact, since the correction factor is a constant. Also if $\phi \approx 0$ or $D_E \leq 0$, this error is negligible. Finally, if the error is noticeable and the position of L_4 is fixed (D_E = constant), $\Delta q'$ might be reduced to zero by locating the mirror M_H at a distance q' from L_4.

This development was supported by grant 1 R01 EY01031 from the Department of Health, Education, and Welfare. The authors acknowledge the contributions of Lloyd Alterton and Carroll Steele of Stanford Research Institute to the mechanical and electronic design.

References

1. We use the convention, here, of stating refractive power of the eye relative to its power when accommodated for infinity, that is, 0.0 diopters of refractive power means that the retina is conjugate with infinity, at 2.0 diopters, the retina is conjugate with a plane 1/2.0 m away, etc. The absolute refractive power of a normal eye accommodated for infinity is about 60 diopters (i.e., its equivalent focal length is about 17 mm).
2. H. D. Crane, and T. N. Cornsweet, J. Opt. Soc. Am. **60**, 577 (1970).
3. The position of CR' is determined by the fact that the image of the eye pupil must be located in the focal plane of L_3 to ensure constancy of brightness and image size independent of the position of L_4.

OFFICE OF NAVAL RESEARCH

Code 442

TECHNICAL REPORTS DISTRIBUTION LIST

OSD

CDR Paul R. Chatelier
Office of the Deputy Under Secretary of Defense
OUSDRE (E&LS)
Pentagon, Room 3D129
Washington, DC 20301

Department of the Navy

Engineering Psychology Programs
Code 442
Office of Naval Research
800 North Quincy Street
Arlington, VA 22217 (5 cys)

Communication & Computer Technology Programs
Code 240
Office of Naval Research
800 North Quincy Street
Arlington, VA 22217

Manpower, Personnel, and Training Programs
Code 270
Office of Naval Research
800 North Quincy Street
Arlington, VA 22217

Information Systems Program
Code 443
Office of Naval Research
800 North Quincy Street
Arlington, VA 22217

Physiology & Neuro Biology Program
Code 441
Office of Naval Research
800 North Quincy Street
Arlington, VA 22217

Special Assistant for Marine Corps Matters
Code 100M
Office of Naval Research
800 North Quincy Street
Arlington, VA 22217

Commanding Officer
ONR Eastern/Central Regional Office
ATTN: Dr. J. Lester
Building 114, Section D
666 Summer Street
Boston, MA 02210

Commanding Officer
ONR Branch Office
ATTN: Dr. C. Davis
1030 East Green Street
Pasadena, CA 91106

Commanding Officer
ONR Western Regional Office
ATTN: Dr. E. Gloye
1030 East Green Street
Pasadena, CA 91106

Office of Naval Research
Scientific Liaison Group
American Embassy, Room A-407
APA San Francisco, CA 96503

Director
Naval Research Laboratory
Technical Information Division
Code 2627
Washington, DC 20375 (6 cys)

Dr. Robert G. Smith
Office of the Chief of Naval Operations, OP987H
Personnel Logistics Plans
Washington, DC 20350

Dr. Jerry C. Lamb
Combat Control Systems
Naval Underwater Systems Center
Newport, RI 02840

Naval Training Equipment Center
ATTN: Technical Library
Orlando, FL 32813

Human Factors Department
Code N215
Naval Training Equipment Center
Orlando, FL 32813

Dr. Alfred F. Smode
Training Analysis and Evaluation Group
Naval Training Equipment Center
Code N-00T
Orlando, FL 32813

Dr. Albert Colella
Combat Control Systems
Naval Underwater Systems Center
Newport, RI 02840

Dr. Gary Poock
Operations Research Department
Naval Postgraduate School
Monterey, CA 93940

Dean of Research Administration
Naval Postgraduate School
Monterey, CA 93940

Mr. Paul Heckman
Naval Ocean Systems Center
San Diego, CA 92152

Mr. Warren Lewis
Human Engineering Branch
Code 8231
Naval Ocean Systems Center
San Diego, CA 92152

Dr. Robert French
Naval Ocean Systems Center
San Diego, CA 92152

Dr. Ross L. Pepper
Naval Ocean Systems Center
Hawaii Laboratory
P.O. Box 997
Kailua, HI 96734

Dr. A.L. Slafkosky
Scientific Advisor
Commandant of the Marine Corps
Code RD-1
Washington, DC 20380

Mr. Arnold Rubinstein
Naval Material Command
NAVMAT 0722 - Rm. 508
800 North Quincy Street
Arlington, VA 22217

Commander
Naval Air Systems Command
Human Factors Programs
NAVAIR 340F
Washington, DC 20361

Commander
Naval Air Systems Command
Crew Station Design
NAVAIR 5313
Washington, DC 20361

Mr. Phillip Andrews
Naval Sea Systems Command
NAVSEA 0341
Washington, DC 20362

Commander
Naval Electronics Systems Command
Human Factors Engineering Branch
Code 4701
Washington, DC 20360

CDR Robert Biersner
Naval Medical R&D Command
Code 44
Naval Medical Center
Bethesda, MD 20014

Dr. Arthur Bachrach
Behavioral Sciences Department
Naval Medical Research Institute
Bethesda, MD 20014

Dr. George Moeller
Human Factors Engineering Branch
Submarine Medical Research Lab
Naval Submarine Base
Groton, CT 06340

Head
Aerospace Psychology Department
Code L5
Naval Aerospace Medical Research Lab
Pensacola, FL 32508

Dr. James McGrath
CINCLANT FLT HQS
Code 04E1
Norfolk, VA 23511

Dr. Robert Blanchard
Navy Personnel Research and Development Center
Command and Support Systems
San Diego, CA 92152

Dr. Julie Hopson
Human Factors Engineering Division
Naval Air Development Center
Warminster, PA 18974

Mr. Jeffrey Grossman
Human Factors Branch
Code 3152
Naval Weapons Center
China Lake, CA 93555

Human Factors Engineering Branch
Code 1226
Pacific Missile Test Center
Point Mugu, CA 93042

Mr. J. Williams
Department of Environmental Sciences
U.S. Naval Academy
Annapolis, MD 21402

Human Factors Section
Systems Engineering Test Directorate
U.S. Naval Air Test Center
Patuxent River, MD 20670

Human Factor Engineering Branch
Naval Ship Research and Development Center, Annapolis Division
Annapolis, MD 21402

CDR W. Moroney
Code 55MP
Naval Postgraduate School
Monterey, CA 93940

Department of the Army

Mr. J. Barber
HQS, Department of the Army
DAPE-MBR
Washington, DC 20310

Dr. Joseph Zeidner
Technical Director
U.S. Army Research Institute
5001 Eisenhower Avenue
Alexandria, VA 22333

Director, Organizations and Systems Research Laboratory
U.S. Army Research Institute
5001 Eisenhower Avenue
Alexandria, VA 22333

Department of the Army (continued)

Technical Director
U.S. Army Human Engineering Labs
Aberdeen Proving Ground, MD 21005

ARI Field Unit-USAREUR
ATTN: Library
C/O ODCSPER
HQ USAREUR & 7th Army
APO New York 09403

Department of the Air Force

U.S. Air Force Office of Scientific Research
Life Sciences Directorate, NL
Bolling Air Force Base
Washington, DC 20332

Chief, Systems Engineering Branch
Human Engineering Division
USAF AMRL/HES
Wright-Patterson AFB, OH 45433

Air University Library
Maxwell Air Force Base, AL 36112

Dr. Earl Alluisi
Chief Scientist
AFHRL/CCN
Brooks AFB, TX 78235

Foreign Addressees

Director, Human Factors Wing
Defence & Civil Institute of Environmental Medicine
Post Office Box 2000
Downsview, Ontario M3M 3B9
CANADA

Dr. A.D. Baddeley
Director, Applied Psychology Unit
Medical Research Council
15 Chaucer Road
Cambridge, CB2 2EF
ENGLAND

Other Government Agencies

Defense Technical Information Center
Cameron Station, Bldg. 5
Alexandria, VA 22314 (12 cys)

Dr. Craig Fields
Director, System Sciences Office
Defense Advanced Research Projects Agency
1400 Wilson Blvd.
Arlington, VA 22209

Dr. Lloyd Hitchcock
Federal Aviation Administration
ACT 200
Atlantic City Airport, NJ 08405

Dr. M. Montemerlo
Human Factors & Simulation Technology, RTE-6
NASA HQS
Washington, DC 20546

Other Organizations

Dr. Jesse Orlansky
Institute for Defense Analyses
400 Army-Navy Drive
Arlington, VA 22202

Dr. T.B. Sheridan
Department of Mechanical Engineering
Massachusetts Institute of Technology
Cambridge, MA 02139

Dr. Arthur I. Siegel
Applied Psychological Services, Inc.
404 East Lancaster Street
Wayne, PA 19087

Dr. Harry Snyder
Department of Industrial Engineering
Virginia Polytechnic Institute and *State University*
Blacksburg, VA 24061

Dr. W.S. Vaughan
Oceanautics, Inc.
422 6th Street
Annapolis, MD 21403

Dr. Robert T. Hennessy
NAS - National Research Council
2101 Constitution Ave., N.W.
Washington, DC 20418

Dr. M.G. Samet
Perceptronics, Inc.
6271 Varial Avenue
Woodland Hills, CA 91364

Dr. Robert Williges
Human Factors Laboratory
Virginia Polytechnic Institute and State University
130 Whittemore Hall
Blacksburg, VA 24061

Dr. Alphonse Chapanis
Department of Psychology
The Johns Hopkins University
Charles and 34th Streets
Baltimore, MD 21218

Journal Supplement Abstract Service
American Psychological Association
1200 17th Street, NW
Washington, DC 20036 (3 cys)

Dr. Christopher Wickens
University of Illinois
Department of Psychology
Urbana, IL 61801

Dr. Babur M. Pulat
Department of Industrial Engineering
North Carolina A&T State University
Greensboro, NC 27411

Dr. Richard W. Pew
Information Sciences Division
Bolt, Beranek & Newman, Inc.
50 Moulton Street
Cambridge, MA 02238

Dr. David J. Getty
Bolt, Beranek & Newman, Inc.
50 Moulton Street
Cambridge, MA 02238

Dr. Douglas Towne
University of Southern California
Behavioral Technology Laboratory
3716 S. Hope Street
Los Angeles, CA 90007

Dr. Stanley N. Roscoe
New Mexico State University
Box 5095
Las Cruces, NM 88003

Dr. William R. Uttal
Institute for Social Research
University of Michigan
Ann Arbor, MI 48109

Dr. Robert Fox
Vanderbilt University
Department of Psychology
Nashville, TN 37240

END

DATE
FILMED

2-82

DTIC